TECHNISCHE UNIVERSITÄT WIEN

Diplomarbeit

3D Structuring of Biocompatible Hydrogels by Means of 2-Photon Polymerization

Zur Erlangung des akademischen Grades

Diplom-Ingenieur

Im Rahmen des Studiums

Technische Physik

eingereicht von

Stefan Binder

Matrikelnummer 01125952

Ausgeführt am Institut für Angewandte Physik
der Fakultät für Physik der Technischen Universität Wien
(in Zusammenarbeit mit dem Institut für Werkstoffwissenschaft und Werkstofftechnologie)

Betreuung
Betreuer: Univ.Prof. Dipl.-Ing. Dr.techn. Gerhard Schütz
Zweitbetreuer: Univ.Prof. Dr.rer.nat. Aleksandr Ovsianikov

Wien, im Jänner 2020 _____ _____

(Unterschrift Verfasser) (Unterschrift Betreuer)

Die approbierte gedruckte Originalversion dieser Diplomarbeit ist an der TU Wien Bibliothek verfügbar.
The approved original version of this thesis is available in print at TU Wien Bibliothek.

Kurzfassung

2-Photon Polymerisation (2PP) ist eine hochauflösende 3D-Druck Technologie, basierend auf der Interaktion von ultrakurzen Laserpulsen mit speziellen photosensitiven Materialien. Aufgrund der nichtlinearen Natur des 2-Photon Absorptionsprozesses kann eine räumliche Auflösung im sub-mikrometer Bereich erzielt werden. Biomedizinische Anwendungen von 2PP sind von besonderem Interesse, da die Technologie es ermöglicht Mikrostrukturen aus verschiedenen Gewebetypen zu produzieren. In dieser Hinsicht erweisen sich Hydrogele als besonders attraktive Materialklasse, da sie es ermöglichen Strukturen in der Gegenwart von lebenden Zellen zu produzieren.

Das Ziel dieser Arbeit war es eine neuartige Klasse von auf Gelatine und Hyaluronsäure basierenden Materialen für 2PP zu etablieren und ihre Zusammensetzung, als auch ihre Verarbeitungsparameter zu optimieren um eine hohe Durchsatzrate zu ermöglichen. Die Zusammenstellung wurde im Weiteren auf ihre Tauglichkeit für die Produktion von hochauflösenden 3D Strukturen in der Gegenwart von lebenden Zellen getestet. Die Analyse von 3D Hydrogelstrukturen wird hauptsächlich durch optische und Laser-Scanning-Mikroskope bewerkstelligt. Informationen über die mechanischen Eigenschaften der mit 2PP produzierten Konstrukte, wurden durch die Analyse des Aufquellverhaltens gewonnen. Diese Methode wurde unter der Zuhilfenahme von automatischer Bilderkennung optimiert.

Die approbierte gedruckte Originalversion dieser Diplomarbeit ist an der TU Wien Bibliothek verfügbar.
The approved original version of this thesis is available in print at TU Wien Bibliothek.
TU Bibliothek Your knowledge hub WIEN

Abstract

2-Photon polymerization (2PP) is a high-resolution 3D printing technology relying on the interaction of ultra-short laser pulses with specialized photosensitive materials. Due to the nonlinear nature of the 2-Photon absorption process spatial resolution in the sub-micrometer range can be achieved. Biomedical applications of 2PP are of particular interest, since this technology is capable of reproducing the microstructure of different tissue types. In this regard, hydrogels represent an especially attractive class of materials, since they potentially allow to produce 3D constructs in the presence of living cells.

The aim of this work is to establish a novel class of gelatin- and hyaluronic acid-based materials for 2PP and optimize their composition as well as processing parameters in order to enable high-throughput fabrication. The formulations will be further tested for their suitability to produce high-resolution 3D structures in the presence of living cells. The main analysis tools for 3D hydrogel structures are optical and laser scanning microscopy. A method to gain information about the mechanical properties of 2PP-produced constructs by the analysis of their swelling behavior was optimized by the use of image recognition.

Die approbierte gedruckte Originalversion dieser Diplomarbeit ist an der TU Wien Bibliothek verfügbar.
The approved original version of this thesis is available in print at TU Wien Bibliothek.
TU Bibliothek Your knowledge hub WIEN

Acknowledgement

I would like to use this opportunity to express my gratitude to those who supported me during my studies and especially during this thesis.

First of all, I would like to thank my supervisors Gerhard Schütz and Aleksandr Ovsianikov for giving me the opportunity to work in this interesting field. It was a great experience to be able to work in such an interdisciplinary group for the first time.

My special thanks go to my colleagues at the Research Group for 3D Printing and Biofabrication, who always offered their support when it was needed. I would like to express my thanks to Marica Markovic and Agnes Dobos for their help during my cell encapsulation experiments and for teaching me a lot about cell culture. Furthermore, I want to thank Franziska Gantner, who helped me understand the intricacies of 2-Photon Polymerization.

I also want to thank my friends, especially those who I got to know as fellow physics student and with whom I spent countless hours studying. Without them I would have never gotten this far.

Finally, I want to express my gratitude to my mother for providing me with support and continuous encouragement throughout my years of study and my life in general.

Die approbierte gedruckte Originalversion dieser Diplomarbeit ist an der TU Wien Bibliothek verfügbar.
The approved original version of this thesis is available in print at TU Wien Bibliothek.
TU Bibliothek Your knowledge hub WIEN

Table of Contents

Die approbierte gedruckte Originalversion dieser Diplomarbeit ist an der TU Wien Bibliothek verfügbar.
The approved original version of this thesis is available in print at TU Wien Bibliothek.
TU Bibliothek Your knowledge hub WIEN

Die approbierte gedruckte Originalversion dieser Diplomarbeit ist an der TU Wien Bibliothek verfügbar.
The approved original version of this thesis is available in print at TU Wien Bibliothek.
TU Bibliothek Your knowledge hub WIEN

1 Introduction

Cells exhibit altered behavior when they are cultured in Petri dishes instead of the far more complex structures of their natural environment. For example, when they are grown in a two-dimensional layer, they can display slower and less efficient growth or even completely different behavior than in three-dimensional scaffolds [1]. To be able to get results from cell culture that are applicable to in-vivo cells, it is therefore important to be able to create environments that closely resemble the extracellular matrix. One novel way to create such scaffolds is 2-photon polymerization (2PP) [2]. 2PP is a CAD-based 3D printing technology that is able to create structures with sub-micron feature size. 2PP uses 2-photon absorption at the focal point of a high-power femtosecond laser beam to initiate polymerization. Due to the non-linear nature of this process, the polymerization is closely confined to the space around the focal point. This means that, while other additive manufacturing technologies like stereolithography require layer-by-layer deposition of material, with 2PP it is possible to produce structures directly in a volume of material. Previously the high resolution of 2PP systems came with the drawback of long fabrication times, which made them ill-suited for work with living cells [3]. However, advance in the technology has led to an increase in writing speed of several magnitudes and speeds of 1000 mm/s are now possible [4].

To utilize 2PP for biofabrication, materials that are biocompatible and simultaneously processable with 2PP, are needed. One class of material, which unites those two requirements, are hydrogels. Hydrogels are highly hydrated networks of polymer chains, that can closely resemble the extracellular matrix [5]. The density of crosslinking between the polymer chains can be adapted by changing the material composition, which enables the tuning of the hydrogel's stiffness within a wide range. This can be used to directly influence growth and other behavior of encapsulated cells [6].

This thesis explores the option to change the hydrogel stiffness not only by modifying the composition, but by varying parameters of the 2PP process, like writing speed and laser power. This would enable the manufacturing of complex structures in which the cell behavior can be influenced based on the cells position, and for example pattern the hydrogel into precisely shaped sections with high and low material stiffness.

Die approbierte gedruckte Originalversion dieser Diplomarbeit ist an der TU Wien Bibliothek verfügbar.
The approved original version of this thesis is available in print at TU Wien Bibliothek.
TU Bibliothek Your knowledge hub WIEN

2 Objective and Approach

The aim of this thesis was to examine the stiffness of two hydrogels based on gelatin and hyaluronic acid in relation to printing speed, laser power, and material composition. Instead of directly measuring the stiffness with an atomic force microscope (AFM), an indirect way of measuring the swelling properties was chosen. One of the main objectives was to streamline the whole testing process to enable a quick testing of many different parameter combinations. To do so, a python program was written for the fast and automatic analysis of confocal laser scanning microscopy (CLSM) images, by using image recognition to measure the size of printed structures.

Additionally, the biocompatibility of the tested hydrogels and its connection to material stiffness was researched by encapsulation of adipose-derived stem cells in the hydrogels.

Die approbierte gedruckte Originalversion dieser Diplomarbeit ist an der TU Wien Bibliothek verfügbar.
The approved original version of this thesis is available in print at TU Wien Bibliothek.
TU Bibliothek Your knowledge hub WIEN

3 Theoretical Background

3.1 Polymerization

Polymerization is the process of small molecules, called monomers, being linked together to macromolecules, which are termed polymers. Since this describes a wide field of different reactions, polymers can be categorized by various means. The two most common classifications are the division based on the polymer structure into condensation and addition polymers and the classification into step- and chain-growth polymerizations, which is based on the polymerization mechanism [7].

Condensation and addition polymers are differentiated by the comparison of the molecular structure of the polymer and the monomers from which it is formed. Condensation polymer are formed with the elimination of small molecules, like for example water. Therefore, some of the atoms which are present in the monomer's molecular formula are missing in the polymer. In contrast, addition polymers are molecule chains with subsegments, which have the same molecular structure as the monomers [8].

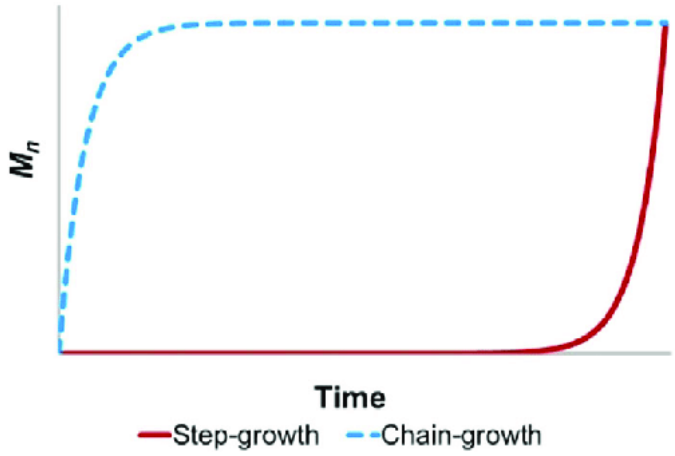

Figure 3.1: Comparison of Chain-growth and Step-growth polymerization; Molecular weight as a function of time [9]

There are also significant differences in the mechanisms by which polymers are formed. Step-growth polymerization starts by two monomers reacting to form a dimer, which can then build a trimer with a monomer or a tetramer with another dimer and so forth. The characteristic property of this kind of reaction is that polymer chains of various length are present during the whole polymerization process and all of them can

Die approbierte gedruckte Originalversion dieser Diplomarbeit ist an der TU Wien Bibliothek verfügbar.
The approved original version of this thesis is available in print at TU Wien Bibliothek.
TU Bibliothek Your knowledge hub WIEN

react with each other [7]. The average molecular weight stays low for most of the reaction and rises sharply at the end (Figure 3.1).

The opposite of this is chain polymerization which is initiated by an active center, for example a radical, and quickly adds hundreds of monomers to a chain. During the process only high molecular weight polymers and monomers are present, while the medium sized polymers which can be found during step-growth polymerization are absent [8]. This leads to a much faster rise of the average molecular weight (Figure 3.1).

One way to create the radical needed to start the reaction is the exposure of a so called photoinitator (PI) to light. In the case of one-photon absorption, the photon energy required for this process usually lies in the UV or visible light range [10]. For 2-photon absorption lower energies are used.

3.2 1-Photon Polymerization

1-photon absorption (1PA) is a process in which a single photon is absorbed by an atom and thereby excites the atom to a higher energy state. The probability of 1PA is a linear function of the light intensity and energy is therefore continuously deposited along the light path. Manufacturing processes that use 1PA to initiate polymerization are called 1-photon polymerization (1PP). The exponential decrease of light intensity in a medium in combination with the linearity of 1PA confines 1PP to surface layers of the material, which makes a layer by layer approach necessary [11].

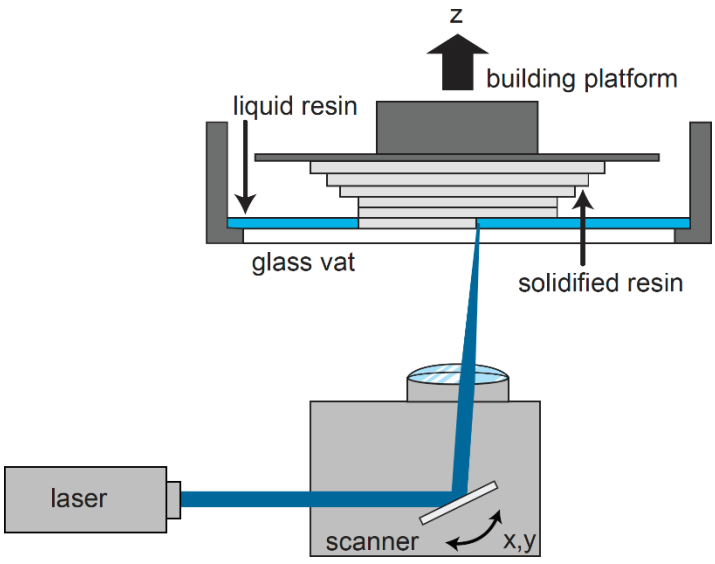

Figure 3.2: schematic setup of a stereolithography manufacturing system [12]

Die approbierte gedruckte Originalversion dieser Diplomarbeit ist an der TU Wien Bibliothek verfügbar.
The approved original version of this thesis is available in print at TU Wien Bibliothek.

One additive manufacturing technique that uses 1PP is stereolithography. In stereolithography a computer-controlled laser beam or a digital light projector is used to selectively illuminate sections of a liquid resin's surface. This induces the polymerization and cures the resin according to the light pattern. The solid structure, which adheres to a movable platform, is then wetted with fresh unpolymerized material and the next layer of resin is cured [13].

3.3 2-Photon Absorption

Multi-photon Absorption (MPA) is the mechanism which leads to the excitation of an atom into a higher energy state by simultaneous absorption of multiple photons. The sum of the photons' energies is the energy difference between the old and new state and neither photon could have excited the atom alone as its energy would be too low. This process was first described by Göppert-Mayer in 1931 [14]. The first demonstration of the effect was realized by Kaiser and Garret in the 1961, a few years after lasers were first available [15]. To observe MPA the photons must interact with the atom within a very short timeframe, which can only be achieved with light sources that show high intensities, such as (pulsed) lasers.

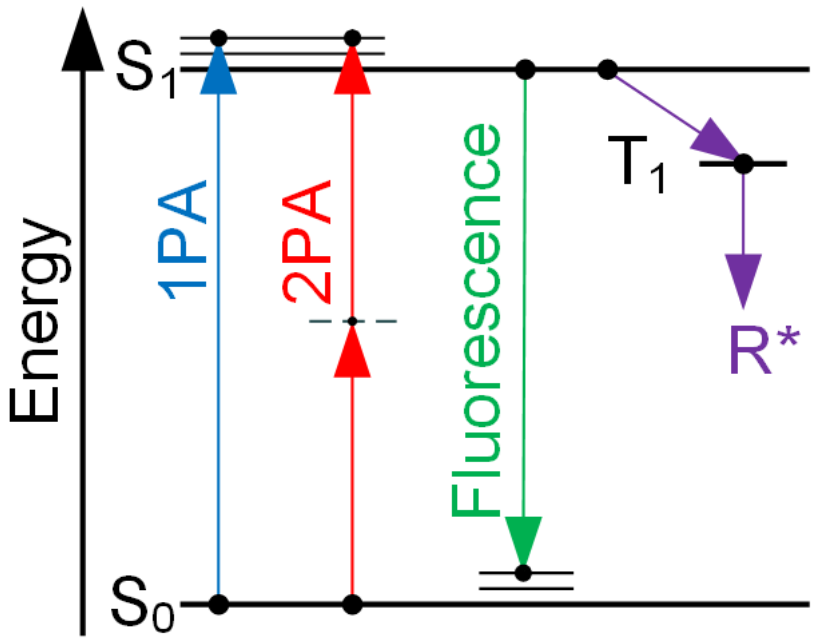

Figure 3.3: Jablonski diagram of single-photon and two-photon absorption [16]

The simplest version of MPA is 2-photon absorption (2PA). In practical applications both photons have the same energy, each half of the energy required to reach the

Die approbierte gedruckte Originalversion dieser Diplomarbeit ist an der TU Wien Bibliothek verfügbar.
The approved original version of this thesis is available in print at TU Wien Bibliothek.
TU Bibliothek Your knowledge hub WIEN

excited atom state, since they are created by the same laser source [17]. A common way to explain this phenomenon is that the first photon creates a virtually state and the second photon has to interact with the atom within the lifetime of this virtual state [18]. After the absorption the atom behaves the same as after 1PA and the absorption can result in fluorescence or formation of a radical (Figure 3.3).

2PA is a non-linear process and its probability increases with the square of the intensity. Due to the high intensity requirement the light source for 2PA has to be a pulsed laser. A pulsed laser can provide high peak power, while keeping the average power low. Additionally, the laser beam has to be focused and 2PA will only occur at the focal point where the intensity is the highest (Figure 3.4) [4].

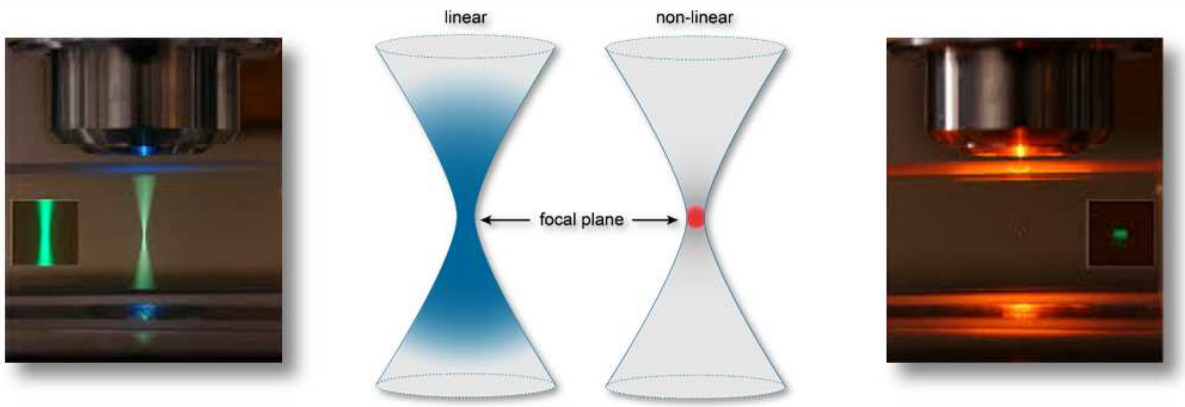

Figure 3.4: Comparison between fluorescence induced by 1PA (left) and 2PA (right) [12] [19]

3.4 2-Photon Polymerization

2-photon polymerization (2PP) is an additive manufacturing process that is characterized by the nonlinear behavior of 2PA. It can be utilized to initiate polymerization at every point in a volume of material instead of just at the surface as in the case of 1PP. When focusing the laser beam in the material with an objective, the polymerized area is confined to the focal point. The exact size of this so-called voxel (volumetric pixel) is determined by the optical components of the system, the laser power and material characteristics. A voxel is only formed if a certain material dependent power threshold is reached. Under this threshold no polymerization will occur. If the laser power is increased above the threshold, the voxel size will also increase until at a certain point certain point destructive thermal effects occur, leading to material damage and bubble formation [12].

Die approbierte gedruckte Originalversion dieser Diplomarbeit ist an der TU Wien Bibliothek verfügbar.
The approved original version of this thesis is available in print at TU Wien Bibliothek.
TU Bibliothek Your knowledge hub WIEN

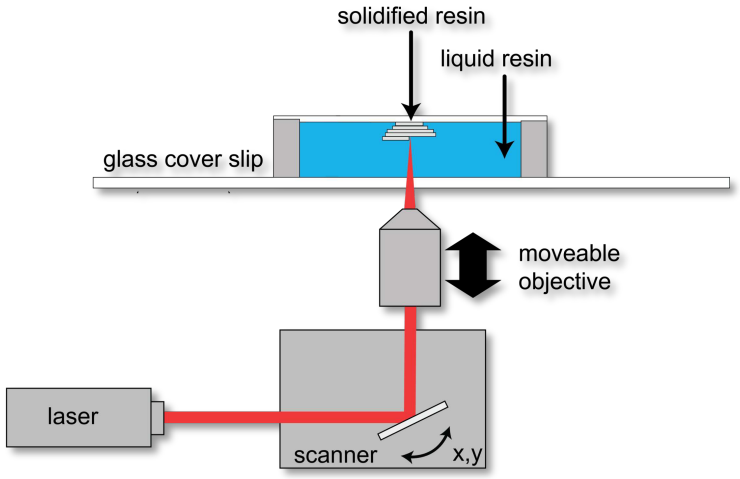

Figure 3.5: schematic setup of a 2PP manufacturing system [12]

2PP manufacturing systems use a laser scanner to shift the laser beam in X and Y direction and adjust the focal point in Z direction by moving the objective. This way microstructures with sub-micron resolution can be fabricated [4].

3.5 Confocal Laser Scanning Microscopy

Confocal Laser Scanning Microscopy (CLSM) is an optical imaging technique, which achieves high resolution along the optical axis, by imaging samples layer by layer and blocking out-of-focus light. This allows for non-invasive imaging of samples with hundreds of µm thickness. In biological and medical science, the main application of CLSM is the imaging of living or fixed samples which have been labelled with fluorescing molecules [20].

In wide-field microscopy the whole field of view (FOV) is illuminated evenly. This leads to an unfocused background being present in the image. To prevent this, in confocal microscopy only one point is illuminated at a time and a pinhole is mounted in the conjugate focal plane to block light from layers other than the original focal plane. To acquire a whole image, the FOV is scanned by the light source and the intensity after the pinhole is measured by a detector. As most of the light is blocked at the pinhole a high initial light intensity is required, which is provided by a laser source. The use of multiple lasers with different wavelength enables the simultaneous excitation of different fluorescent molecules. The different wavelengths of the fluorescence signal can be separated with wavelength-depended filters and guided to multiple sensors [21].

Die approbierte gedruckte Originalversion dieser Diplomarbeit ist an der TU Wien Bibliothek verfügbar.
The approved original version of this thesis is available in print at TU Wien Bibliothek.
TU Bibliothek Your knowledge hub WIEN

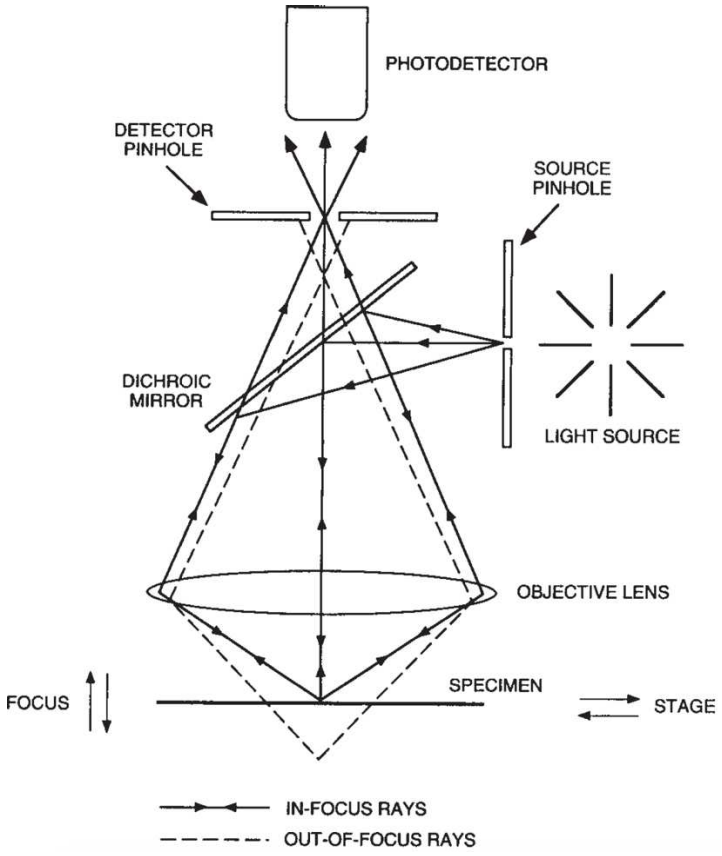

Figure 3.6: Schematic illustration of a LSCM system [20]

Die approbierte gedruckte Originalversion dieser Diplomarbeit ist an der TU Wien Bibliothek verfügbar.
The approved original version of this thesis is available in print at TU Wien Bibliothek.

4 Experimental Setup

4.1 2PP-Setup

The used 2PP-system was developed and built by Peter Gruber in the framework of his dissertation [4]. Figure 4.1 shows a schematic illustration of the 2PP-Setup which is based on a tunable, pulsed high-power femtosecond laser and a number of optical components that direct the laser to the sample: In order to regulate the maximum laser power that enters the setup the polarization of the laser light is controlled by a rotating achromatic waveplate. Followed by a polarizing beam splitter cube that transmits the p-polarized part of the light. The reflected s-polarized part of the laser light is directed into a beam dump.

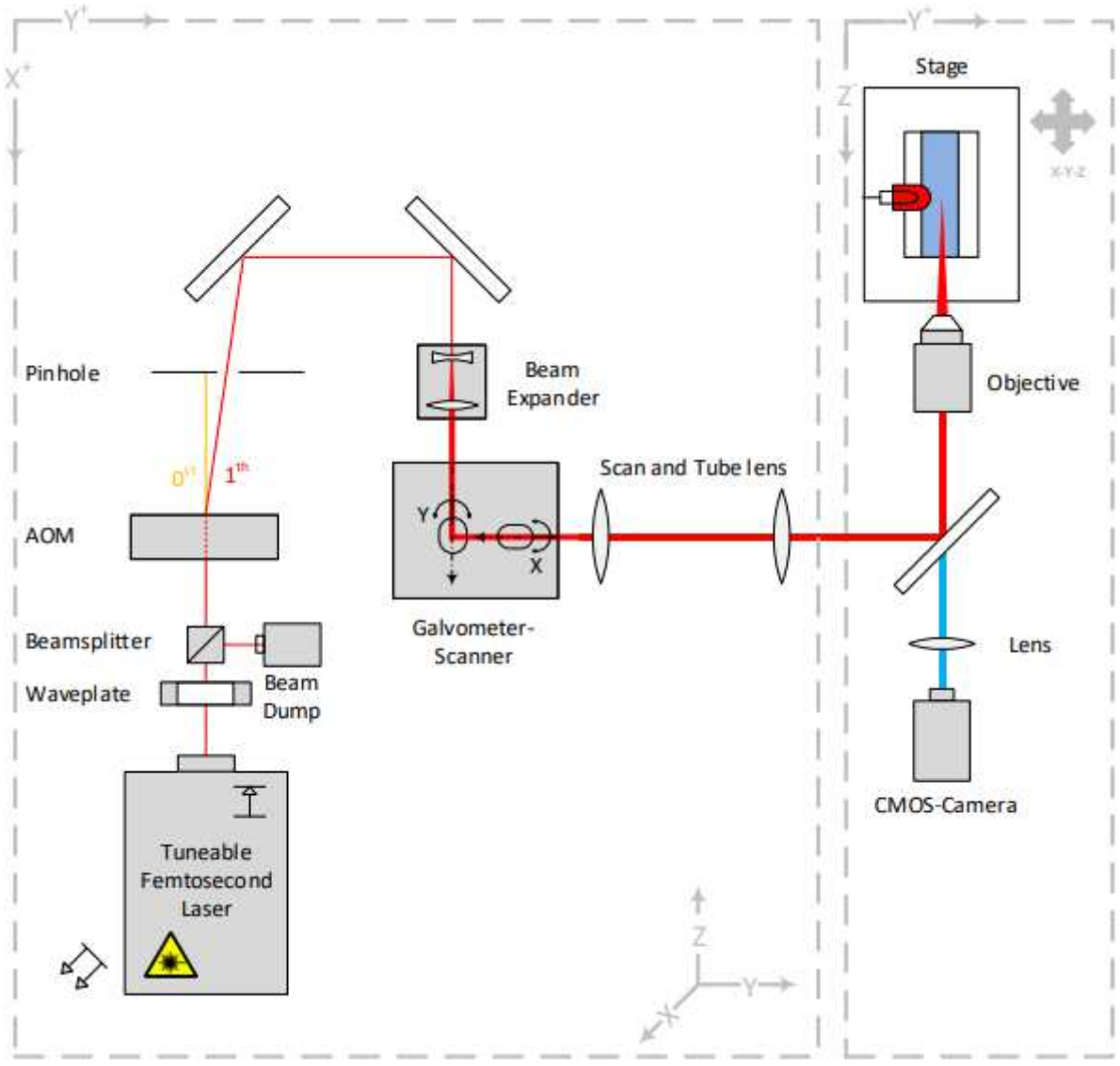

Figure 4.1: Schematic of the 2PP-Setup [4]

Die approbierte gedruckte Originalversion dieser Diplomarbeit ist an der TU Wien Bibliothek verfügbar.
The approved original version of this thesis is available in print at TU Wien Bibliothek.

An acousto-optic modulator (AOM) enables a fast power modulation during the structuring process. The zero-order beam is blocked after the AOM by a pinhole through which only the first order beam can pass. With this configuration a fast modulation of the beam in the range of MHz can be achieved, a speed that cannot be reached by optical shutters.

Before the Galvanometer-Scanner a 5x achromatic beam expander (GBE05-B, Thorlabs, Newton, USA) is mounted to expand the laser beam to subsequently overfill the rear aperture of the objective. This leads to a smaller focal spot and therefore higher resolution. The Galvanometer-Scanner is used to shift the beam in the XY-plane. After the scanner an optical system composed of two achromatic lenses and an objective is mounted, allowing it to take full advantage of the scanners angular range. An objective focuses the laser beam into the sample. Two linear positioning stages move the objective in Z-direction and the sample in XY-direction. A CMOS-Camera mounted under the objective behind a semi-transparent mirror allows to observe the sample during printing.

4.1.1 Tunable High-Power Laser

A diode-pumped solid state femtosecond Ti:Sapphire laser (MaiTai eHP DeepSe) is used as the laser source for the setup. It is tunable from 690 nm to 1040 nm and offers a typical pulse duration of 70 fs with a repetition rate of 80 MHz. The average output power is 2,9 W, which categorizes the laser as a class IV laser (IEC 60825-1). Since required the output-power for the 2PP-Setup is only about 500 mW, most of it is directed to a beam dump by a beam splitter (PBS052, Thorlabs) directly after the laser. The ratio is controlled by a λ/2-waveplate (467-4210, Eksma Optics).

4.1.2 Acousto-optic modulator

An AOM (MT110-B50A1.5-IR, AA-Opto-Electronic) was used as a switch for the laser beam and to modulate the laser power. The AOM consists of a transparent crystal, which is connected to a piezoelectric transducer. By applying an oscillating electrical signal to the transducer, an acoustic wave is generated in the crystal, which is equivalent to a periodic local change of the refractive index. When a laser beam passes through the crystal it is partially diffracted at this refractive index grating. The diffraction efficiency is dependent on the wavelength of the laser beam, the input angle of the

Die approbierte gedruckte Originalversion dieser Diplomarbeit ist an der TU Wien Bibliothek verfügbar.
The approved original version of this thesis is available in print at TU Wien Bibliothek.
TU Bibliothek Your knowledge hub WIEN

beam and the frequency of the electrical signal. Switching times are limited by the speed of sound in the crystals and are in the order of 10^{-7} s. The zero-order beam is blocked by a beam, while the first passes on to the Galvanometer-Scanner.

4.1.3 Galvanometer-Scanner

The galvanometer-scanner (intelliSCAN 10, Scanlab AG) deflects the laser beam in the XY-plane, by using two mirrors, which are each connected to a galvanometer. When using a 10x objective the scanner can reach marking speeds of up to 1000mm/s, while maintaining high accuracy.

4.1.4 Optical System

Positioning the scanner directly in front of the objective, would lead to a severely limited scanning angle since the laser power decreases for larger angles. To achieve a large and uniform structuring area, a setup with two additional lenses, similar to the one in a CLSM, was chosen. These lenses are called scan lens and tube lens and are positioned in a so-called '4f' arrangement.

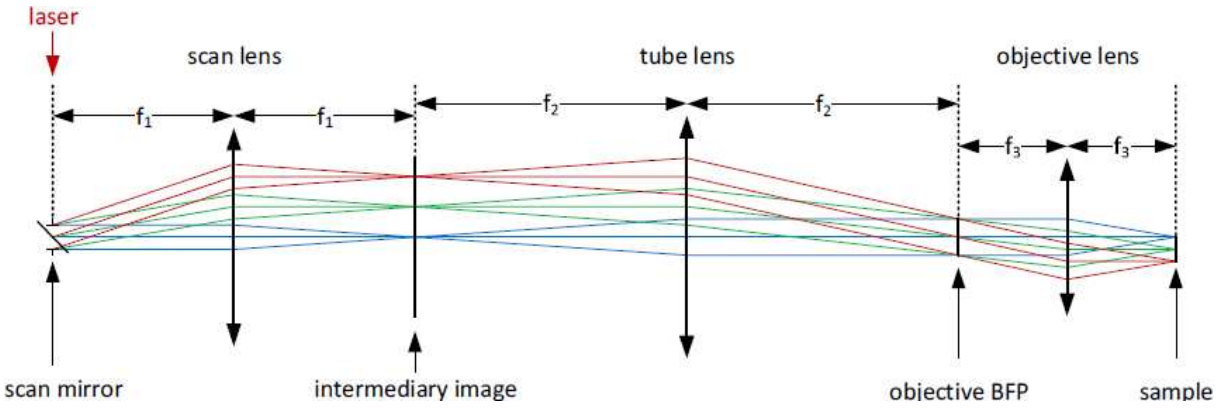

Figure 4.2: "4f" arrangement of scanner, lenses and objective [4]

The scan lens is positioned in a way that its focal plane lies between the two mirrors of the scanner. The distance between the scan lens and the tube lens is the sum of their focal lengths. The objective is then placed with its back focal plane in the focal plane of the tube lens. Due to their different focal lengths the scan lens (f = 100 mm) and the tube lens (f = 150 mm) also serve as a beam expander. This ensures that the rear aperture of the objective is completely filled by the laser beam.

Die approbierte gedruckte Originalversion dieser Diplomarbeit ist an der TU Wien Bibliothek verfügbar.
The approved original version of this thesis is available in print at TU Wien Bibliothek.
TU Bibliothek Your knowledge hub WIEN

For the experiments described in this thesis only a Super-Achromat 10x/0.4 objective (Olympus) was used. The 10x magnification enables fast writing speeds while the numerical aperture is still high enough to achieve high-definition details.

4.1.5 Stage

The structuring area that can be covered by the galvanometer-scanner is restricted by the FOV of the objective. Therefore, a linear positioning stage (SCANplus IM 120 x 80, Märzhäuser), which can shift the sample in XY-direction is used to build bigger structures or fabricate objects over an area larger than the FOV. Position changes in the Z-direction are achieved by a second stage onto which the objective is mounted. The stages are equipped with stepper motors which offer a high number of microsteps and therefore a high positioning accuracy.

Die approbierte gedruckte Originalversion dieser Diplomarbeit ist an der TU Wien Bibliothek verfügbar.
The approved original version of this thesis is available in print at TU Wien Bibliothek.
TU Bibliothek Your knowledge hub WIEN

5 Materials

All chemicals and cells were purchased from Sigma-Aldrich (Saint Louis, USA) unless stated otherwise.

5.1 Hydrogels

Hydrogels are crosslinked networks of polymer chains, which are hydrophilic and therefore contain high amounts of water. By using materials, which also are present in the extracellular matrix (e.g. hyaluronic acid or collagen), hydrogels can be tailored to be excellent environments for 3D cell culture [1]. For 2PP manufacturing the crosslinking process must be efficient, quick and controllable. This is accomplished by using thiol-ene reactions. Radical-mediated thiol-ene reactions are step-growth click reactions, with high reactivity, which can be photoinitiated and form homogeneous polymer networks [22].

Two Hydrogels based on thiol-ene photo-click chemistry were used for the experiments in this thesis.

5.1.1 GelNB

Gelatin is a naturally abundant biopolymer, which exhibits great cell compatibility, but dissolves at temperatures needed for a cell culture environment. To adapt gelatin for photo-crosslinking applications, the material is modified with highly reactive norbornene functionalities. Norbornene, compared to other functionalities like for example acrylates, offers the advantage that no homopolymerization will occur and it undergoes efficient step-growth polymerization when crosslinked with a thiolated crosslinker [22].

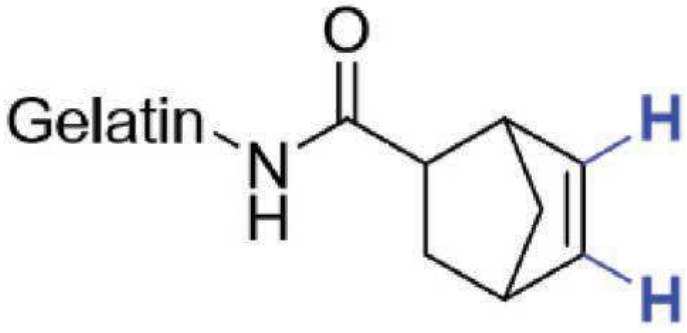

Figure 5.1: Molecular structure of GelNB [22]

Die approbierte gedruckte Originalversion dieser Diplomarbeit ist an der TU Wien Bibliothek verfügbar.
The approved original version of this thesis is available in print at TU Wien Bibliothek.
TU Bibliothek Your knowledge hub WIEN

Gelatin–Norbornene (GelNB) was synthesized [22] and provided by the Polymer Chemistry and Biomaterials Group at the Ghent University.

5.1.2 NorHA

Hyaluronic acid is one of the main components of the extracellular matrix and has a major influence on cell proliferation and migration. This makes it an excellent base material for hydrogels, which are intended to mimic the natural cell environment. Norbornene-functionalized hyaluronic acid (NorHA) can be crosslinked with di-thiols to form non-toxic hydrogels. It has previously been shown that by varying the thiol/norbornene ratio of the reaction, the stiffness of the hydrogel can be changed within a wide range [6]. This makes it an ideal candidate to test if the stiffness can be influenced by adjusting printing parameters during the 2PP structuring process.

NorHA was synthesized [6] and provided by the group of Prof. Burdick from the Department of Bioengineering at the University of Pennsylvania (Philadelphia, USA).

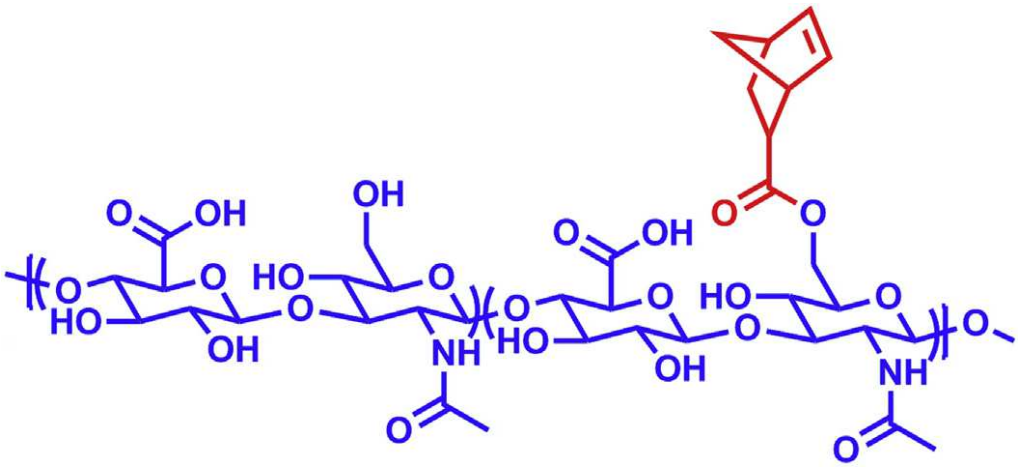

Figure 5.2: Molecular structure of NorHA; ~20% of the hyaluronic acid (blue) repeat units are functionalized with norbornene (red) [6]

5.1.3 DTT

Dithiothreitol (DTT) is a di-thiol and was used as crosslinker for both types of hydrogels. All experiments were performed with an equimolar thiol/norbornene ratio unless stated otherwise.

Die approbierte gedruckte Originalversion dieser Diplomarbeit ist an der TU Wien Bibliothek verfügbar.
The approved original version of this thesis is available in print at TU Wien Bibliothek.
TU Bibliothek Your knowledge hub WIEN

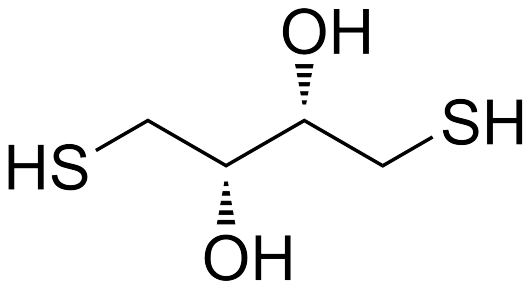

Figure 5.3: Molecular structure of DTT

5.2 Photoinitiator

A diazosulfonate-based photoinitiator (DAS) was used to start the crosslinking reaction. While a higher concentration of DAS compared to its predecessor P2CK is needed to reach the same 2PP-structuring performance, DAS exhibits superior biocompatibility and is therefore well suited for cell encapsulation [23]. DAS was stored as a 10 mM stock solution and used with a concentration of 0.5 mM in the hydrogels.

DAS was developed by Maximilian Tromayer in the framework of his dissertation [23] and was synthesized at the Institute of Applied Synthetic Chemistry (TU Wien).

5.3 FITC-Dextran

Dextran labelled with fluorescein isothiocyanate (FITC-Dextran) is a fluorescent agent. For the experiments in this thesis FITC-dextran with a molecular weight of 2000 kDa (TdB Consultancy AB, Uppsala, Sweden) was used in a concentration of 0,05 mg/ml. Due to the large size of these molecules, FITC-dextran is not able to penetrate polymerized hydrogels and can therefore be used to create an inversed image of the 2PP-printed hydrogel structures.

5.4 Functionalization of Coverslips

To ensure that the printed structures adhere to the glass surface of the coverslips, the glass was functionalized with methacrylate groups. The functionalization was performed according to the following instructions:

- The coverslips were plasma cleaned to provide a contaminant free surface for an even distribution of the methacryalte groups.
- A stock solution of 100ml was prepared with the following compounds:

Die approbierte gedruckte Originalversion dieser Diplomarbeit ist an der TU Wien Bibliothek verfügbar.
The approved original version of this thesis is available in print at TU Wien Bibliothek.
TU Bibliothek Your knowledge hub WIEN

Table 5.1: Stock solution compounds

Ethanol 98% - technical grade	48 ml
Distilled water	50 ml
Acetic Acid glacial ≥ 99.85 % Sigma 537020	0,3 ml
3-(Trimethoxysilylpropyl)-methacrylate Sigma 440159	2 ml

The trimethoxysilylpropyl methacrylate was added dropwise over the course of 3 minutes under stirring. The solution was stirred for 30 minutes.

- The coverslips were incubated in the stock solution for 45 minutes.
- Afterwards, the coverslips were cleaned with distilled water and put in an oven at 110 °C for 30 minutes to dry.

5.5 Adipose-derived Stem Cells

Immortalized human adipose-derived mesenchymal stem cells were purchased from Evercyte, Vienna, Austria (ASC/TERT1) and labelled with green fluorescent protein (ASC-GFP). Labelled cells were used for the cell encapsulation experiments in this thesis to remove the need for staining before imaging, which makes the process easier and faster. The disadvantage is that this approach makes it more challenging to image the printed cubes and cells simultaneously, because GFP and FITC-dextran are fluorescent in the same spectral range.

Cells were cultured and maintained in Endothelial Cell Growth Medium-2 (EGM-2) from Lonza, Basel, Switzerland, supplemented with fetal bovine serum (FBS) (Sigma-Aldrich, Saint Louis, MO, USA) to a final concentration of 10%. Cells were incubated in a humidified atmosphere with 5% CO_2 at 37°C. At 80% confluence the cells were detached using 0.5% trypsin-EDTA solution (Gibco, Waltham, MA, USA) and after the cells detached serum rich medium was added to inactivate trypsin. The cells were collected in a Falcon tube and centrifuged at 300 rpm for 3 min, resuspended in cell media and eventually seeded onto T75 flasks in a 1:3 ratio.

Die approbierte gedruckte Originalversion dieser Diplomarbeit ist an der TU Wien Bibliothek verfügbar.
The approved original version of this thesis is available in print at TU Wien Bibliothek.
TU Bibliothek Your knowledge hub WIEN

6 Methods

6.1 Swelling Tests

The behavior of cells encapsulated in hydrogels depends on the stiffness of the surrounding hydrogel [24]. Therefore, when a hydrogel is polymerized, usually in an UV chamber, altered cell behavior is achieved by adapting the composition of the hydrogel. For example, by using a lower concentration the resulting polymer network will be less dense and thus less stiff. This method comes with the disadvantage that the behavior cannot be influenced individually in specific areas of the hydrogel. When using 2PP to create hydrogel structures, it is possible to influence the material stiffness by varying the structuring parameters. By regulating the amount of energy that is deposited per voxel the degree of crosslinking can be adjusted and therefore also the stiffness of the hydrogel. This should enable the production of complex structures, within which the cell growth can be confined to certain sections.

The aim of this thesis was to analyze the influence of structuring parameters on the stiffness of hydrogels. One way to measure the stiffness is atomic force microscopy (AFM). However, since AFM measurements would have been very time consuming for the large number of samples that were created during this thesis, an alternative method of measurement, namely the quantification of swelling, was chosen. Lower stiffness means that the material can deform easier and is able to absorb more of the surrounding liquid, which leads to swelling of the structure. Consequently, it is possible to make some conclusions regarding the stiffness of different structures by comparing their swelling. To realize this approach cubes of a size of 300 x 300 x 200 µm were fabricated with various structuring parameters, developed in PBS, incubated and then imaged with a CLSM to measure the size difference and hence the swelling.

6.2 Material Preparation

6.2.1 Hydrogel Preparation

The Hydrogels were prepared directly before starting the printing process according to the following protocol. All volumes and weights necessary for the preparation were

Die approbierte gedruckte Originalversion dieser Diplomarbeit ist an der TU Wien Bibliothek verfügbar.
The approved original version of this thesis is available in print at TU Wien Bibliothek.
TU Bibliothek Your knowledge hub WIEN

calculated in a spreadsheet. An example of these calculations can be found in the appendix.

1. Small amounts of the base material (GelNB or NorHA) and the crosslinker DTT (GelNB: 10-20mg; NorHA: 3-10mg; DTT: 1-4mg) were weight into separate microcentrifuge tubes.
2. The base material was dissolved in PBS. When working with GelNB, the solution was placed in a 40°C heat bath to fully dissolve the GelNB.
3. A DTT stock solution was prepared.
4. Photoinitiator and DTT solution were added to the base material solution. For cell encapsulation experiments, the cells were also added to the material in this step.
5. The finished material was then pipetted into a silicon mold in an ibidi µ-dish. To prevent evaporation during the printing process a glass cover slip was placed on top of the silicon mold.

6.2.1.1 Crystal Formation in NorHA Hydrogel

First tests showed that if NorHA Hydrogel was prepared according to the protocol in chapter 6.2.1, crystals would form during the printing process. Tests with different combinations of the hydrogel components showed that crystal formation only occurred if the photoinitiator was added to the material. The problem was solved by using cell media instead of PBS for the preparation of NorHA hydrogel. Even though a previous pH-test of the material showed no measurable abnormalities, the use of cell medium instead of PBS prevented the formation of crystals. It was hypothesized that this effect was caused by the fact that cell media contains a pH buffer and therefore stabilized the hydrogel's pH value.

Die approbierte gedruckte Originalversion dieser Diplomarbeit ist an der TU Wien Bibliothek verfügbar.
The approved original version of this thesis is available in print at TU Wien Bibliothek.
TU Bibliothek Your knowledge hub WIEN

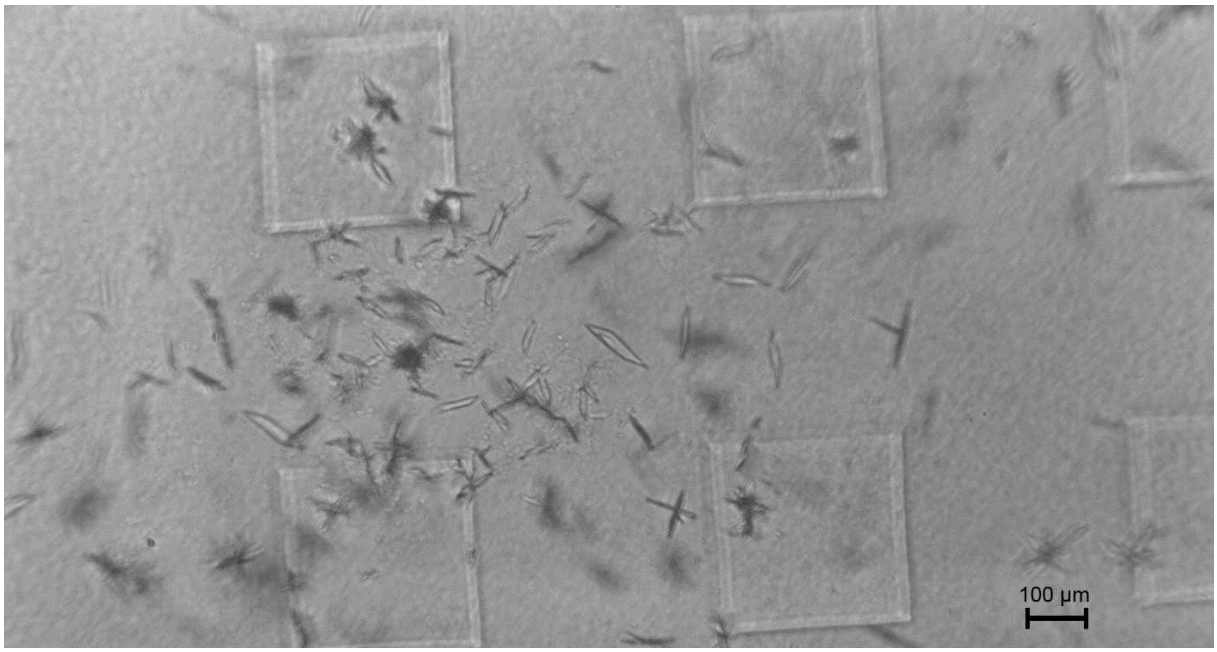

Figure 6.1: Crystal formation in NorHA hydrogel after 90 min printing time. Showing printed structures with crystals inbetween

6.2.2 ASC Preparation

In the case of cell encapsulation experiments, the cells had to be prepared in parallel to the hydrogel. The ASCs were trypsinized, spun down in a centrifuge at 300 rpm for 3 min and resuspended in cell media. To reach a final concentration of 1 million cells per mL, they were then counted, spun down once more and resuspended in the calculated amount of cell media. Cell preparation was taken care of by Marica Markovic and Agnes Dobos.

6.3 Structuring Parameters

The following parameters all affect the printing process and the properties of the resulting structures. The non-linear nature of 2PP makes the interrelations between parameters hard to predict. Therefore, to get a full understanding of the materials, it is often necessary to test a broad set of parameter combinations.

6.3.1 Objective

The choice of objective has a high influence on the structuring process, since different magnification and numerical aperture (NA) result in a different feature size, available field of view, required laser power, and maximum writing speed. For the experiments

Die approbierte gedruckte Originalversion dieser Diplomarbeit ist an der TU Wien Bibliothek verfügbar.
The approved original version of this thesis is available in print at TU Wien Bibliothek.
TU Bibliothek Your knowledge hub WIEN

in this thesis an Olympus objective (Super-Achromat 10x/0.4, Olympus, Tokyo) was used. This enabled high writing speeds of up to 1000 mm/s, while keeping the feature size reasonably small and power requirements low.

6.3.2 Power

To ensure optimal structuring the laser beam output power must be set correctly. The power threshold defines the power under which no structuring is possible and is a function of the other parameters. For short exposure times per voxel (< 1 ms) the threshold scales with the square root of the writing speed. But the threshold does not tend towards zero for longer exposure times, which are equivalent to low writing speeds. This effect is caused by the quenching of radicals by oxygen, which prevents the initiation of the polymerization process [25]. Further an upper limit exists for the useful power range, over which the material can over polymerize, form bubbles or is simply destroyed by thermal effects.

If the power is set within these limits, the structuring will be successful but can show various material properties depending on the used power. In this thesis it was studied how different power settings influence the stiffness of the material. This is based on the theory that when using laser powers close to the threshold, not all available norbornene and thiol groups are crosslinked, which leads to a softer material than structuring with higher power. To test this prediction arrays of cubes with different laser power for each row were printed.

6.3.3 Speed

The speed, with which the laser beam is scanned across the sample, is directly connected to the total structuring time. To keep the fabrication time short a high speed is usually desired. However, since the structuring speed also affects the physical properties of the material, it has to be ensured that a higher writing speed does not lead to unwanted side effects such as a higher power threshold which could lead to destructive thermal effects.

To examine how different structuring speeds affect the material, the cube arrays were printed with 100 mm/s, 500 mm/s and 1000 mm/s.

Die approbierte gedruckte Originalversion dieser Diplomarbeit ist an der TU Wien Bibliothek verfügbar.
The approved original version of this thesis is available in print at TU Wien Bibliothek.
TU Bibliothek Your knowledge hub WIEN

6.3.4 Hatch & Layer Spacing

In each layer in Z-direction the laser beam is directed in lines in either X or Y direction. After each line the beam is moved a certain distance called hatch. Similarly, the layer spacing dZ is the distance by which the sample is moved by the stage in Z-direction. Both setting must be chosen in a way that the voxels of neighboring lines and consecutive layers overlap enough to build a stable structure. Since the printed voxels are elongated in Z-direction dZ can be set much higher than the hatch.

While Hatch and dZ also change the stiffness and other properties of printed structures, their exact influence has not been explored in this thesis due to time constraints.

6.4 Printing Procedure

Ibidi µ-dishes (Martinsried, Planegg, Germany) were used as sample holders and the hydrogel was contained by rubber molds with ~30 or ~150 µl volume and covered by a glass coverslip to prevent evaporation during the printing process. In general printing duration was kept under three hours as the hydrogel's printing characteristics could be compromised during a prolonged printing process and results from different prints would not be comparable. For cell encapsulation experiments printing duration was capped at one hour to prevent unnecessary stress of the cells and potential cell death. All prints were performed at a laser wavelength of 720 nm. After the printing process the unpolymerized material was dissolved with PBS and removed from the sample. After adding ~2ml of PBS, the samples were incubated at 37 °C for at least 24 hours before analysis. Samples from cell experiments were stored with cell media instead of PBS and the cell media was exchanged every 3-4 days.

6.5 Image Acquisition

A Zeiss LSM 800 was used to image the samples. As the used hydrogels are not fluorescent, a FITC-dextran 2000 solution was added to the sample. As the FITC-dextran molecules were not able to diffuse into the hydrogel, only the area surrounding the cubes was fluorescent during imaging, which lead to a negative image of the cubes.

The connection of the bottom part of the printed structures to the glass surface of the sample holder, reduces the swelling in that area. Therefore, the swelling is more pronounced in the top section of the cubes. To be able to measure this difference,

Die approbierte gedruckte Originalversion dieser Diplomarbeit ist an der TU Wien Bibliothek verfügbar.
The approved original version of this thesis is available in print at TU Wien Bibliothek.
TU Bibliothek Your knowledge hub WIEN

multiple images of each sample at varying Z-positions were taken. The Z-stack feature of the Zeiss LSM 800 allowed for this to be done automatically, by simply selecting a region of interest in the Z-direction and setting the step distance.

To make the image acquisition even less time consuming the tiles feature of the microscope was used. An area larger than the FOV in the XY-plane can be selected and the software splits the area into tiles which are consecutively scanned.

6.6 Image Analysis

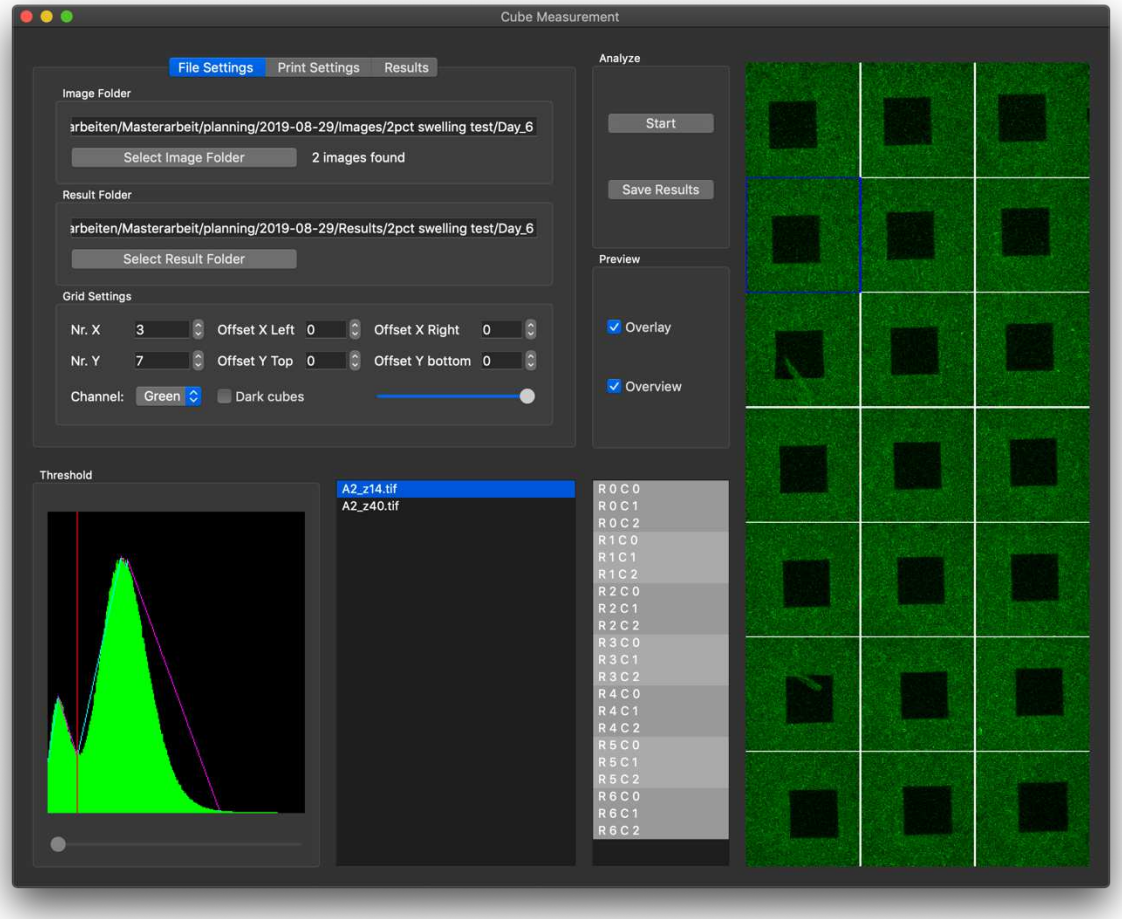

Figure 6.2: GUI of the image analysis program

The most basic way to analyze the images would be to simply manually measure the size of every cube in a graphics editor. This method is not only cumbersome and time consuming, but also prone to mistakes and only reproducible within a certain margin of error. Therefore, a Python program was written to reliably analyze the images. The program was built with a graphical user interface (GUI) (

Die approbierte gedruckte Originalversion dieser Diplomarbeit ist an der TU Wien Bibliothek verfügbar.
The approved original version of this thesis is available in print at TU Wien Bibliothek.
TU Bibliothek Your knowledge hub WIEN

Figure 6.2), to make it more accessible. After entering the folder in which, the images are stored, each image can be selected from a list and viewed within the program. By entering the size of the imaged array, the image is divided into section, each containing one cube. When selecting one of these sections, its histogram will be displayed. After this setup, the automated analysis can be started. The program will then transform each section into a black and white (B&W) image, where the cube is represented as white and the surrounding area as black. Afterwards, an algorithm from a computer vision library finds the contour of the white area and fits bounding rectangle with the smallest possible area to the contour. As its result the measurement then returns the area of the contour, the side lengths of the bounding rectangle and its area. The results are also displayed graphically as overlays of the original image. This enables a fast verification of the measurement. The collected data can be exported into a spreadsheet as raw values. Alternatively, by entering additional parameters of the print, the program will calculate the average values for each row of the structured array and export the processed numbers.

6.6.1 Image Recognition

Although measuring the size of a rectangle in an image seems trivial for a human, it is rather tricky to design a program that manages to fulfil the task in reliable fashion. While the program offers the possibility to manually correct the measurement after the automated analysis, doing so for more than a few of the cubes, would quickly diminish the time savings of using the program instead of manual analysis. Therefore, most of the work on the program went into ensuring that the image recognition works even for images with less than ideal quality.

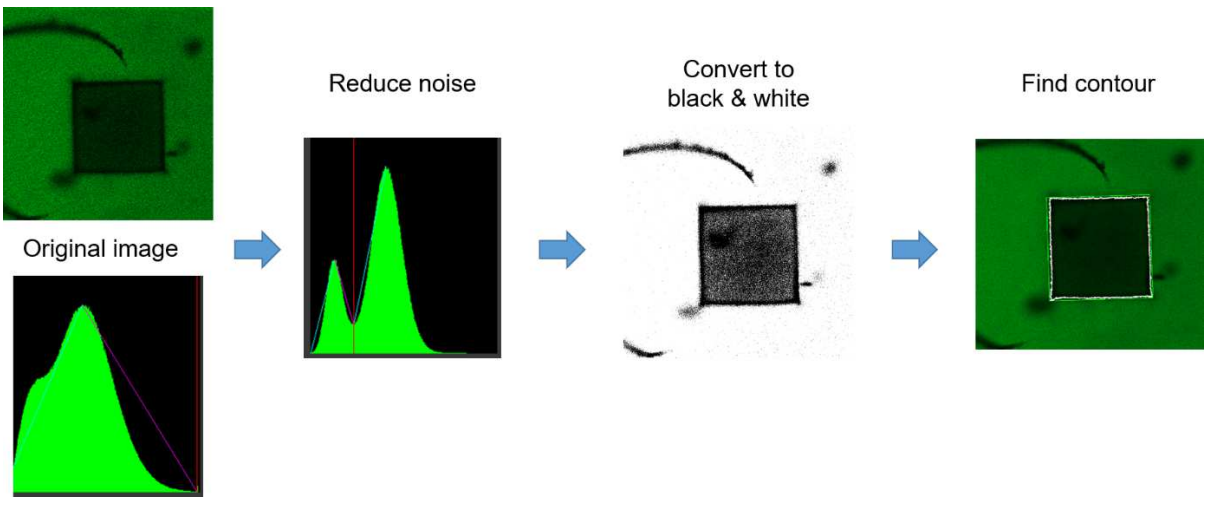

Die approbierte gedruckte Originalversion dieser Diplomarbeit ist an der TU Wien Bibliothek verfügbar.
The approved original version of this thesis is available in print at TU Wien Bibliothek.

Figure 6.3: Image recognition process sequence

For this part of the program multiple functions from the Open source computer vision (OpenCV) library were utilized. The library is originally written in C++, but a Python package is also available. Firstly, for the image recognition to work, the image has to be converted into a binary B&W image, to separate the subject from the background. This is done by selecting on of the color channels, choosing a threshold and setting all pixels with a color value greater than the threshold to 1 and all other pixels to 0. There are multiple ways to choose the threshold. The simplest would be to set a global threshold for the whole image, but this approach does not work if there is an illumination gradient in the image. As CLSM images often show such gradients, for example due to nonhomogeneous distribution, adaptive thresholding is necessary. Adaptive thresholding means that the image is divided into subsections, for each of which its own threshold is calculated. OpenCV offers multiple algorithms for adaptive thresholding, but while these work for a wide range of images, it is harder to enter manual adjustments when they fail, than for a self-written algorithm. Therefore, a compromise between a global threshold and adaptive thresholding was chosen. The image is divided into fairly large sections each containing one cube, and a threshold is calculated for each section. This calculation relies on the histogram. The histogram of an ideal image would only contain two sharp peaks, one for the cube area and one for the background. Noise and uneven illumination lead to a broadening of these peaks into a Gaussian distribution. The minimum between the peaks can be used as the threshold. Due to the high noise level in the raw images the peaks overlap too much to determine a distinct minimum. To reduce the noise, the images are simply downscaled by 50%. This comes with the disadvantage, that the original images have to be fairly large to provide high resolution even after downscaling.

After the images were converted to B&W, an OpenCV function was used to find the boundary of areas of connected pixels with the same color. As the program would not only find the contour of the cubes, but also of impurities in the sample, these were filtered out by dismissing all contours but the largest from each section. The area of these contours is later used to calculate the relative swelling of the cubes. Additionally, the smallest possible bounding rectangle is fitted to the contour. Comparing the area of the contour and the area of the rectangle is a good indicator if any deformations have occurred.

Die approbierte gedruckte Originalversion dieser Diplomarbeit ist an der TU Wien Bibliothek verfügbar.
The approved original version of this thesis is available in print at TU Wien Bibliothek.
TU Bibliothek Your knowledge hub WIEN

7 Results & Discussion

7.1 GelNB

7.1.1 Swelling Behavior

10 w/v% GelNB hydrogel was tested with 100, 500 and 1000 mm/s scanning speed. To roughly determine the power threshold for each of these speeds 10 rows with multiple cubes and increasing laser power for each row were printed. The starting power was 10 mW and increased to 100 mW in 10 mW steps. As was expected, the power threshold required to successfully create stable structures, was lower for lower scanning speeds. As a next step a more precise value was measured by printing a second set of arrays with a power range of 20 mW around the previously determined threshold area and a step size of 2 mW. The thresholds discovered this way can be seen in Table 7.1.

Table 7.1: Power thresholds at different scanning speeds for 10 w/v% GelNB hydrogel

Scanning Speed	Power Threshold
100 mm/s	28 mW
500 mm/s	38 mW
1000 mm/s	46 mW

Analysis of the swelling behavior showed that low laser power leads to higher swelling, but the swelling trends towards a fixed level within 10 to 15 mW above the threshold and stays there for the rest of the measured range (Figure 7.2). This behavior at higher laser power matches closely with the expected behavior of an ideal step-growth hydrogel network [26]. The curves for different scanning speeds seem to only be shifted along the X-axis due to the different thresholds. The 100 mm/s curve appear to show increased swelling above 50 mW, but this upwards trend is in fact caused by overpolymerization of the material and the resulting deformation of the printed structures (Figure 7.1 (b)). The overpolymerized cubes showed a higher size increase in the center of the structure in Z-direction, while the regularly printed cubes exhibited the highest degree of swelling at the top.

Die approbierte gedruckte Originalversion dieser Diplomarbeit ist an der TU Wien Bibliothek verfügbar.
The approved original version of this thesis is available in print at TU Wien Bibliothek.
TU Bibliothek Your knowledge hub WIEN

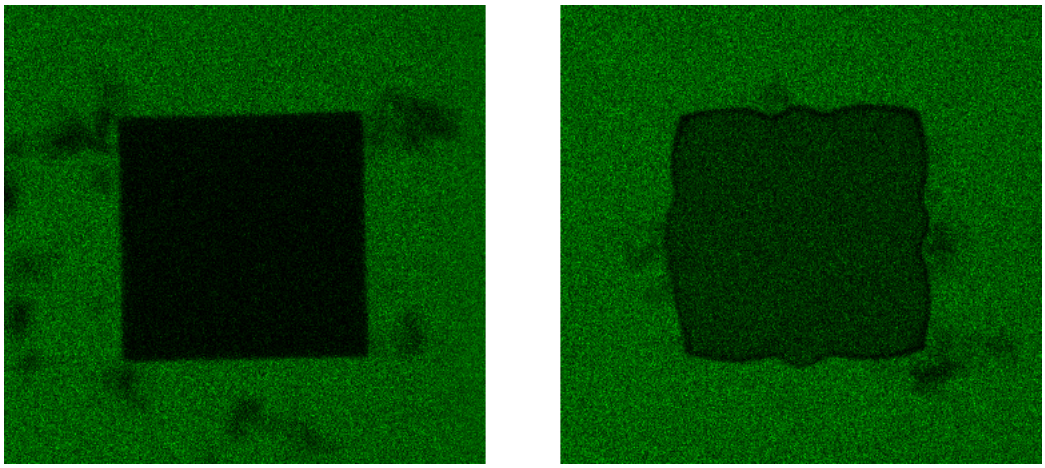

(a) 40 mW (b) 90 mW

Figure 7.1: Comparison of two cubes printed with a speed of 100 mm/s. One cube (a) was structured with 40 mW and retained his original shape, while the other (b), printed with 90 mW, overpolymerized and deformed.

For each cube swelling in top and bottom layer has been measured. The lower swelling of the bottom layers is caused by the material being connected to the glass surface which leads to suppressed swelling.

In Figure 7.2 a certain offset between the series of measurements with 2 mW steps and the ones with 10 mW steps can be seen. The border between the glass cover slip and the printed structures cannot be determined without a certain inaccuracy. Therefore, this imaging method does not allow it to measure the swelling of each sample at the same position in z-direction leading to the offset between measurement series. However, since it does not change the results in a qualitative way the offset was accepted.

To examine how the printing parameters influence on the swelling behavior compared to different material composition, 7,5 w/v% GelNB hydrogel was used to print an array with a scanning speed of 1000 mm/s. Once again, the swelling was higher close to the power threshold and then settled at roughly 40% swelling for higher power settings (Figure 7.3). This value is about twice as high as for the hydrogel with 10 w/v% GelNB, which matches the prediction that the material with less crosslinkable polymers and therefore less dense polymer network should be softer and swell more. The same experiment was attempted with 5 w/v% GelNB hydrogel, but no stable structures could be printed with the material.

Die approbierte gedruckte Originalversion dieser Diplomarbeit ist an der TU Wien Bibliothek verfügbar.
The approved original version of this thesis is available in print at TU Wien Bibliothek.
TU Bibliothek Your knowledge hub WIEN

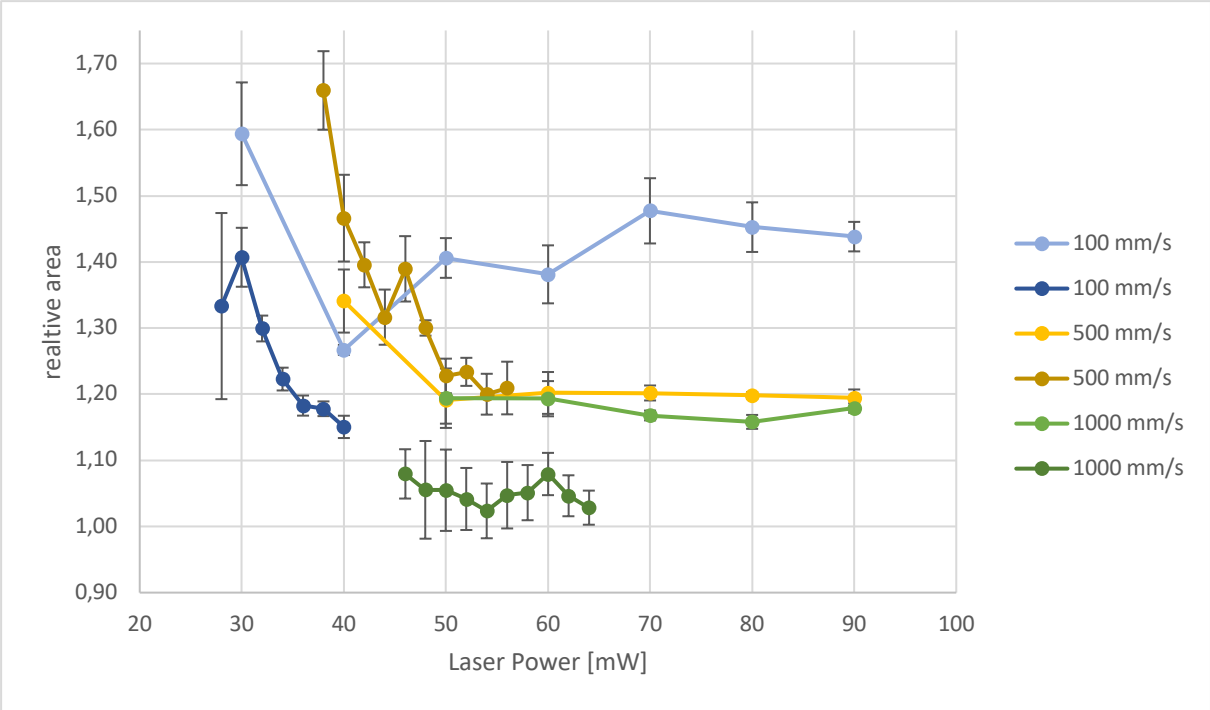

Figure 7.2: Swelling behavior of 10 v/w% GelNB hydrogel structured with different writing speeds. The increased area of structures printed with 100 mm/s and more than 50 mW is caused by overpolymerization. The error bars represent the standard deviation from the mean.

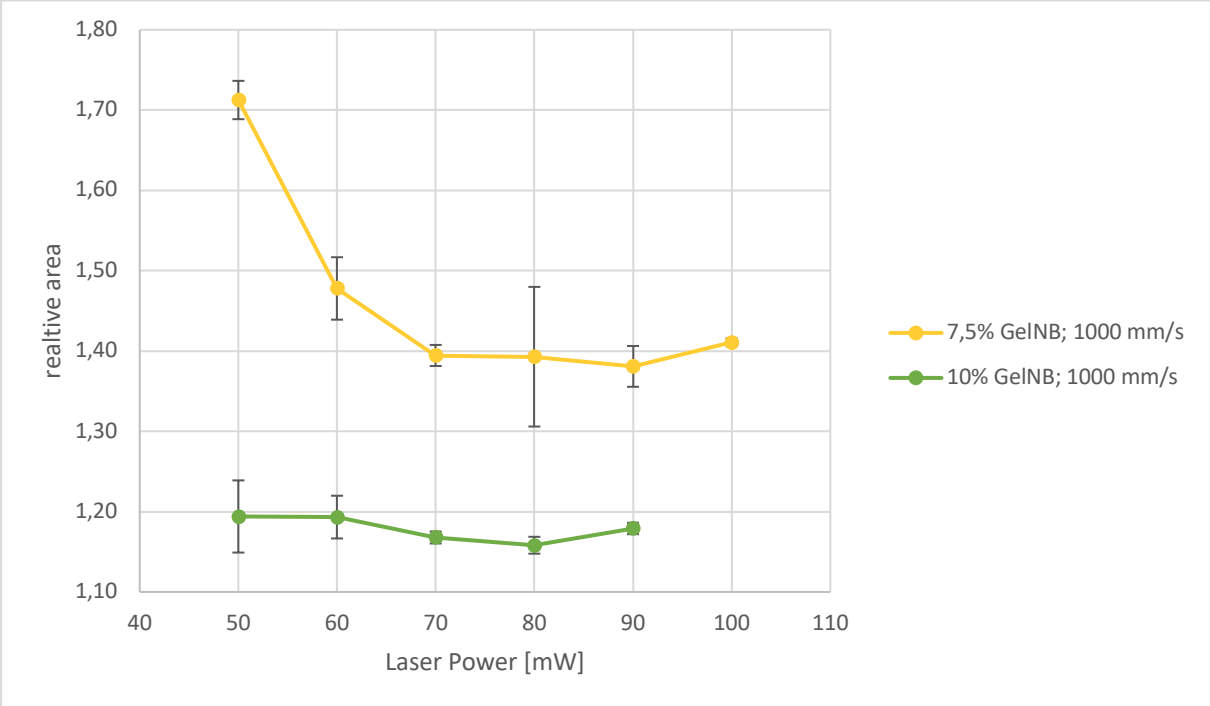

Figure 7.3: Comparison of 7,5 w/v% and 10 w/v% GelNB hydrogel. As predicted the less dense polymer network and thus lower stiffness of the 7,5 w/v% hydrogel results in higher swelling.

Die approbierte gedruckte Originalversion dieser Diplomarbeit ist an der TU Wien Bibliothek verfügbar.
The approved original version of this thesis is available in print at TU Wien Bibliothek.
TU Bibliothek Your knowledge hub WIEN

7.1.2 Cell Encapsulation

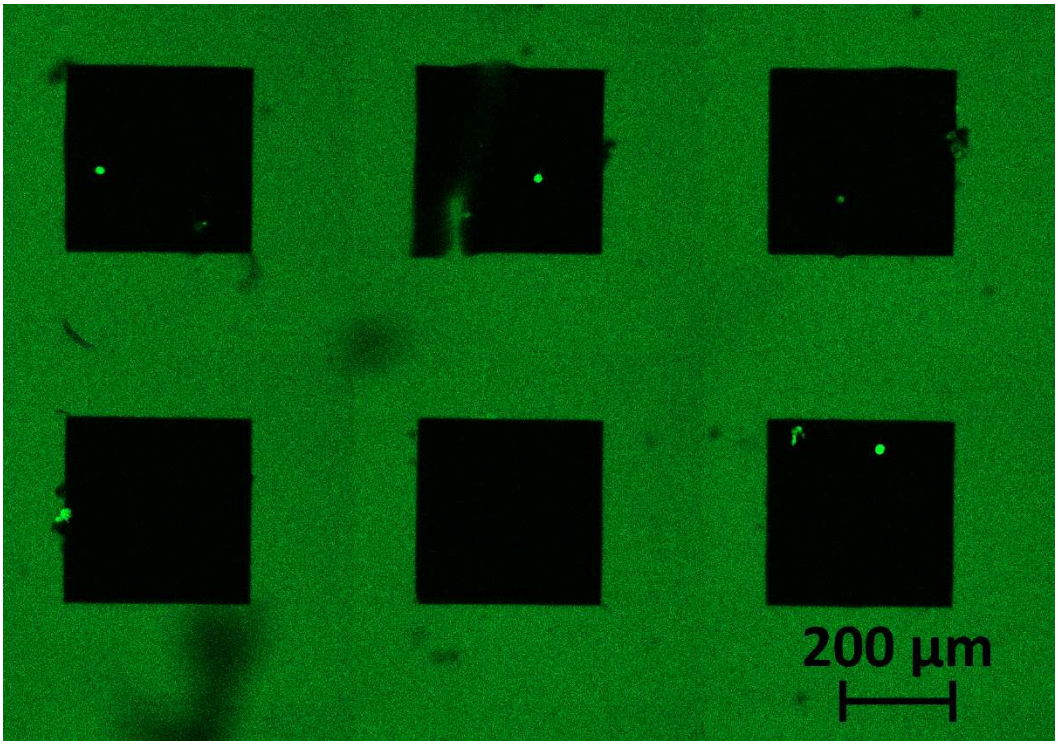

Figure 7.4: ASC-GFP encapsulation in 10 w/v% GelNB hydrogel after 1 day of incubation. Only very few living cells (bright green dots) are left in and around the cubes.

The biocompatibility of both, the hydrogel with 10 w/v% and the one with 7,5 w/v% GelNB, was tested in cell encapsulation experiments. To reduce the fabrication time and thus the stress on the cells, printing was performed only at 1000mm/s scanning speed and two columns of each power step instead of three were printed. This resulted in a total printing time of slightly less than an hour. After 24 hours incubation the 10 w/v% sample contained almost no living cells (Figure 7.4).

Die approbierte gedruckte Originalversion dieser Diplomarbeit ist an der TU Wien Bibliothek verfügbar.
The approved original version of this thesis is available in print at TU Wien Bibliothek.
TU Bibliothek Your knowledge hub WIEN

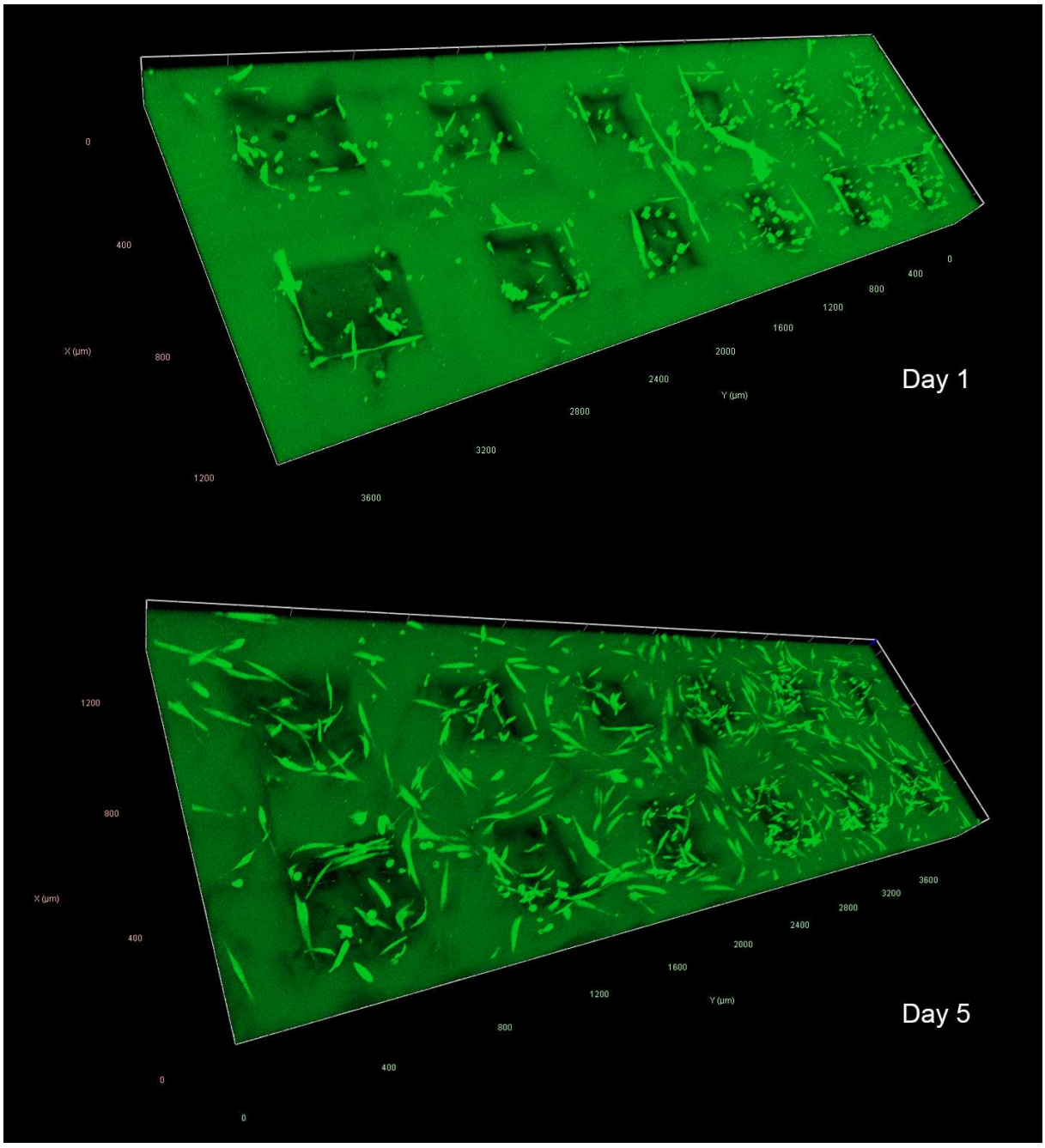

Figure 7.5: ASC-GFPs encapsulated in 7,5 w/v% GelNB hydrogel after 1 day (top) and 5 days (bottom) of incubation. The cubes are displayed as empty space with the surrounding area being fluorescent (dark green) due to FITC-dextran. The GFP-labelled cells can be seen in a brighter green. The two images show growth of the cells in and around the hydrogel structures, indicating good biocompatibility of the material

Meanwhile, in hydrogel with 7,5 w/v% GelNB cell survival inside the printed structures was higher and cells on the glass surface already started to stretch out, indicating high biocompatibility of the material (Figure 7.5, top). After 5 days the cells inside the hydrogel were also stretched out (Figure 7.6) and all cells on the sample showed proliferation (Figure 7.5, bottom). This behavior matches with the results from chapter

Die approbierte gedruckte Originalversion dieser Diplomarbeit ist an der TU Wien Bibliothek verfügbar.
The approved original version of this thesis is available in print at TU Wien Bibliothek.
TU Bibliothek Your knowledge hub WIEN

7.1.1, were a higher degree of swelling and therefore, lower stiffness was observed in the 7,5 w/v% GelNB hydrogel than in the 10 w/v% GelNB hydrogel.

Figure 7.4 and Figure 7.5 show CLSM images of the cell encapsulation experiments. The GFP signal from the ASCs can be seen in bright green, while the background is a darker green due to the use of FITC-dextran. The printed structures are either displayed as black in the 2D images or as empty space in the 3D renderings.

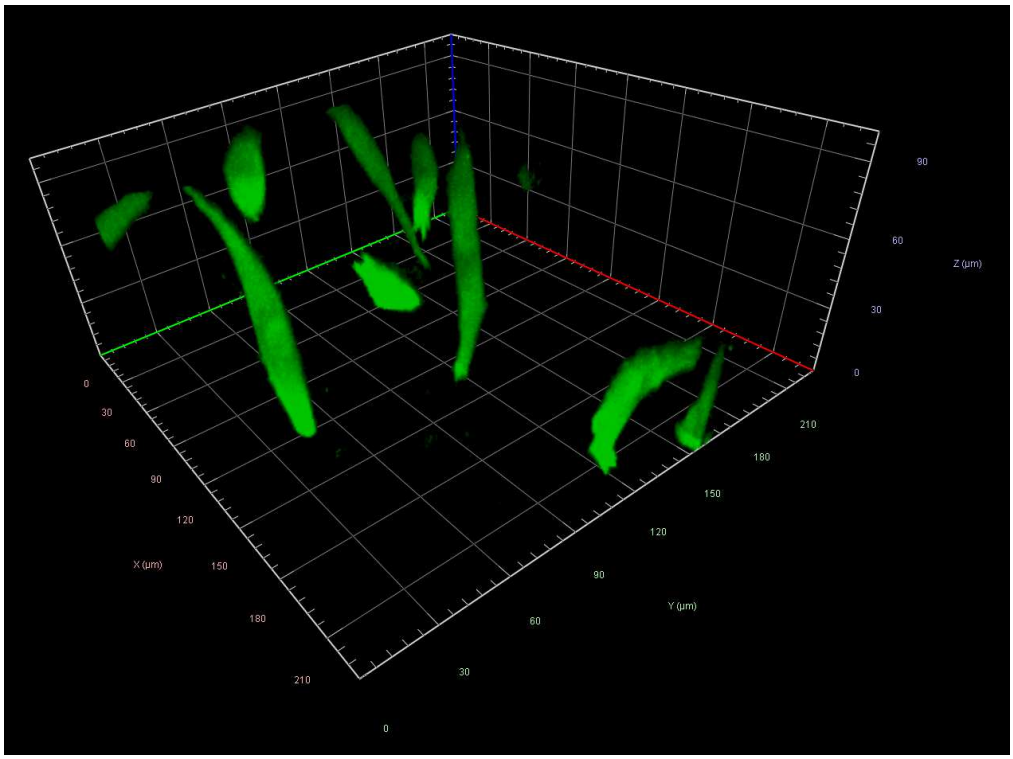

Figure 7.6: ASC-GFPs in a single cube of 7,5 w/v% GelNB hydrogel 5 days after encapsulation. The image shows only the GFP-labelled cells inside a 100 µm high section of the cube, which makes it easier to identify changes in morphology. The cells can clearly be seen to have stretched out since the encapsulation.

7.2 NorHA

7.2.1 Swelling Behavior

NorHA based hydrogel was only printed with a scanning speed of 1000 mm/s, since the experiments with GelNB had already shown, that lower writing speeds offer no additional control over the stiffness. Multiple concentrations from 1 w/v% to 4 w/v% of NorHA were tested and 2%, 3% and 4% were found to result in stable constructs, while 1% and 1,5% could not be structured. For an additional experiment 4 w/v% NorHA hydrogel was used with a lower thiol/norbornene ratio of 0,3.

Die approbierte gedruckte Originalversion dieser Diplomarbeit ist an der TU Wien Bibliothek verfügbar.
The approved original version of this thesis is available in print at TU Wien Bibliothek.
TU Bibliothek Your knowledge hub WIEN

Table 7.2: List of tested NorHA hydrogel compositions and whether they resulted in stable 2PP structures

NorHA concentration	thiol/norbornene ratio	Successful 2PP structuring
4,0%	1,0	Yes
4,0%	0,3	Yes
3,0%	1,0	Yes
2,0%	1,0	Yes
1,5%	1,0	No
1,0%	1,0	No

First tests with an incubation time of 1 day showed similar results as observe with the GelNB hydrogel. The material exhibits higher swelling close to the power threshold, but only slight swelling or even slight shrinkage for powers 15 – 20 mW above the threshold (Figure 7.7). Analysis after 5 days of incubation revealed a different and unexpected behavior. All cubes had shrunk to sizes smaller than the original printing dimensions. Cubes printed with lower power featured less shrinkage while higher laser power led to reduction of the cross-section area of ~30% (Figure 7.8).

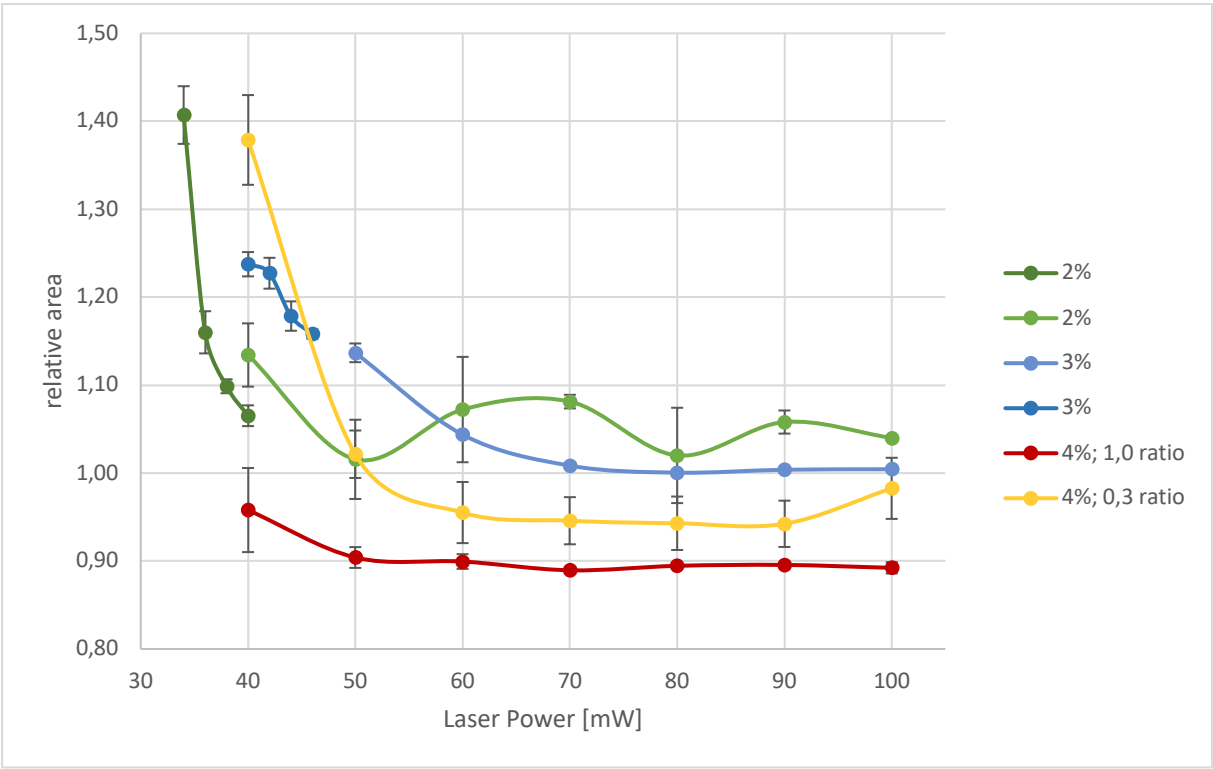

Figure 7.7: Swelling of different compositions of NorHA hydrogel after 1 day of incubation. The structures display swelling of up to 40% at low power, while maintaining their original size at higher power settings

Die approbierte gedruckte Originalversion dieser Diplomarbeit ist an der TU Wien Bibliothek verfügbar.
The approved original version of this thesis is available in print at TU Wien Bibliothek.
TU Bibliothek Your knowledge hub WIEN

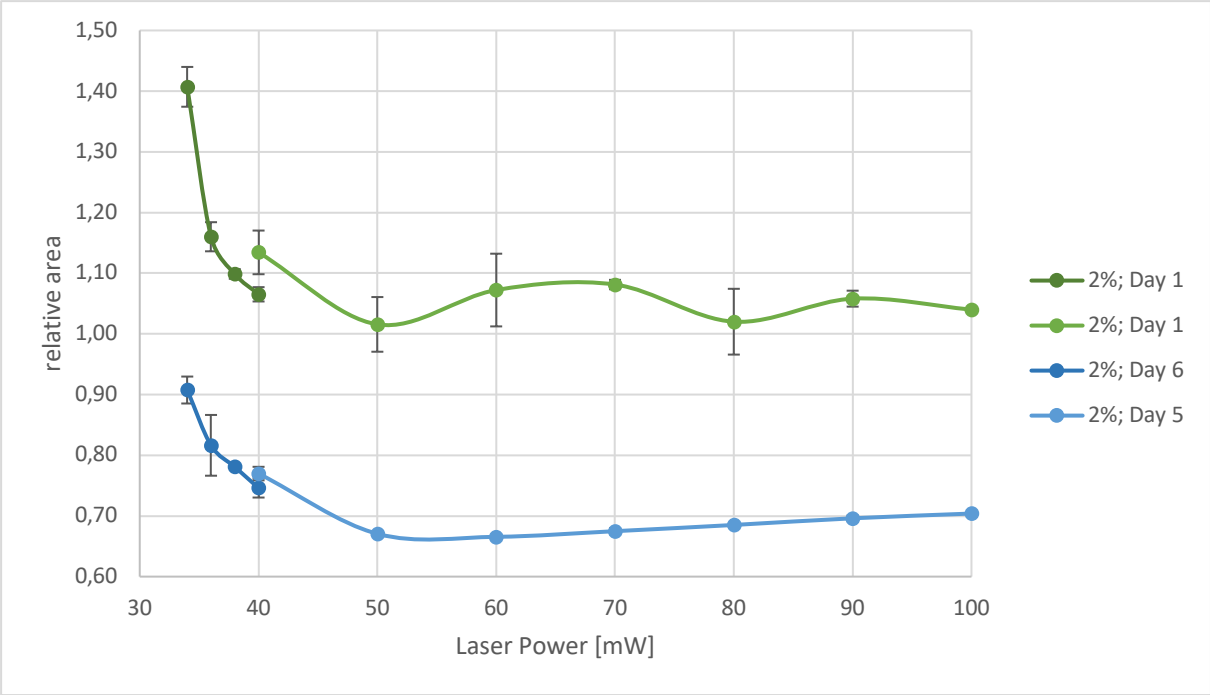

Figure 7.8: Comparison of the swelling behavior of 2 w/v% NorHA hydrogel after 1 and 5 days of incubation. While exhibiting behavior similar to GelNB hydrogel after 1 day, the structures shrink if incubated longer.

The cause of the shrinkage after several days of incubation could not be fully clarified yet. However, two possible explanations are, that it is either caused by contraction of the polymer chains or by a change of hydrophilicity after the crosslinking process. Both hypotheses would explain the lower shrinkage of the cubes fabricated with lower laser powers. With lower intensities polymer networks that are less crosslinked are created, thus showing less shrinkage compared to fully crosslinked structures.

7.2.2 Cell Encapsulation

2PP cell encapsulation experiments were conducted with 2 w/v% and 4 w/v% NorHA hydrogel. Both concentrations lead to comparable results. The cells on the glass surface and on top of the printed cubes showed a high degree of proliferation even after 1 day of incubation. One sample showed such high cell growth, that after 7 days most of the cubes had been ripped off the glass and pulled in between the last 4 cubes connected to the surface (Figure 7.10), indicating great biocompatibility of the hydrogel, which leads to high cell proliferation. In contrast to this, the cells inside the structures showed no signs of proliferation and kept the round morphology (Figure 7.9). This is consistent with previously published results, which showed that cells seeded

Die approbierte gedruckte Originalversion dieser Diplomarbeit ist an der TU Wien Bibliothek verfügbar.
The approved original version of this thesis is available in print at TU Wien Bibliothek.
TU Bibliothek Your knowledge hub WIEN

on top of high stiffness NorHA hydrogel displayed increased spreading with increased stiffness, while cells inside the hydrogel exhibited the opposite behavior [24].

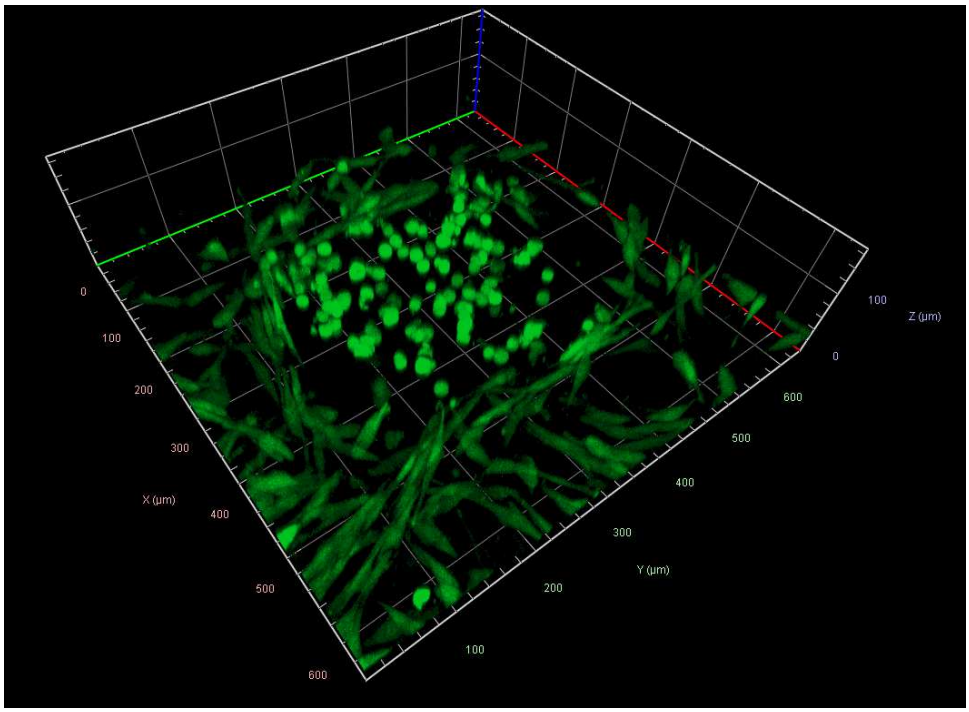

Figure 7.9: CLSM image of static cells inside a single cube and proliferating cells in the surrounding area after 1 day of incubation

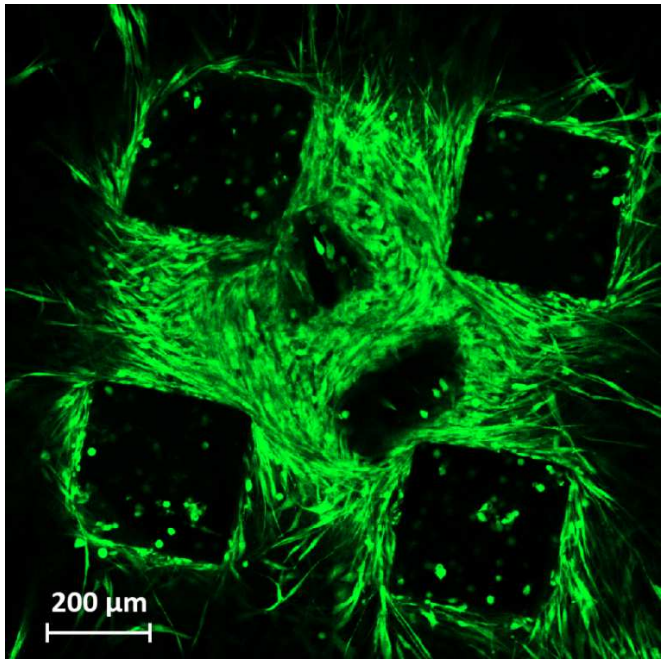

Figure 7.10: Highly proliferating cells with ripped off cubes in the center

Die approbierte gedruckte Originalversion dieser Diplomarbeit ist an der TU Wien Bibliothek verfügbar.
The approved original version of this thesis is available in print at TU Wien Bibliothek.
TU Bibliothek Your knowledge hub WIEN

To see if proliferation inside the hydrogel is possible at low stiffness, three UV cell encapsulation experiments were performed. All three samples had a NorHA concentration of 1,5 v/w% and thiol/norbornene ratios of 1,0, 0,45 and 0,12.

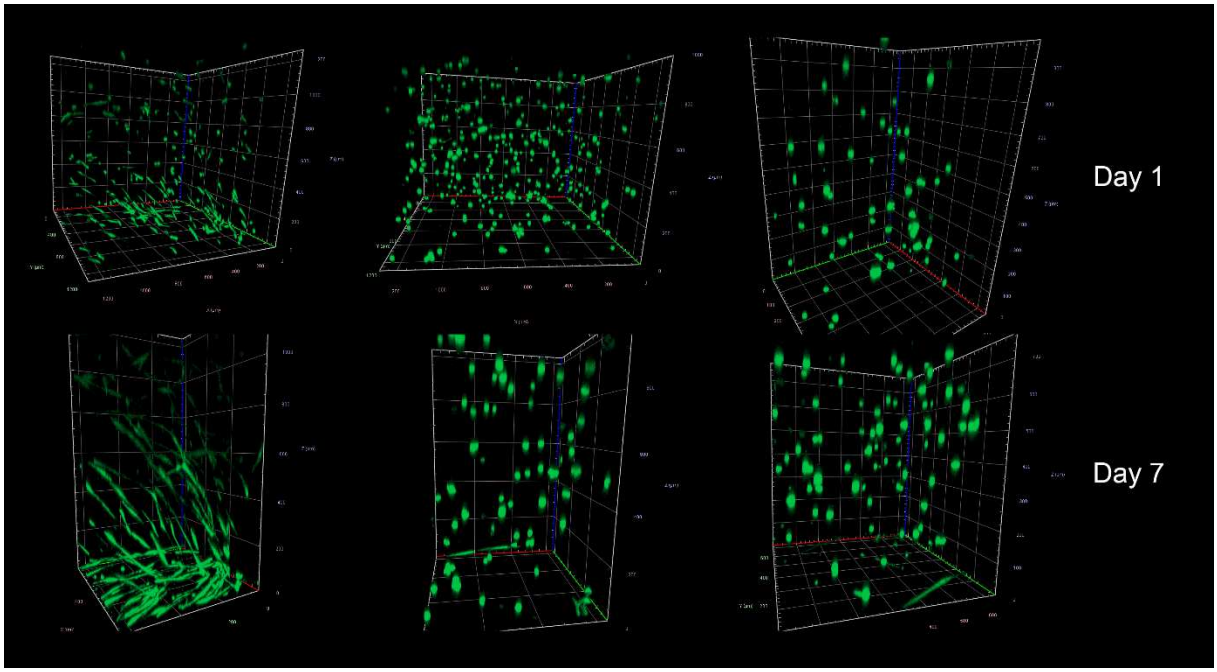

Figure 7.11: UV cell encapsulation of ASC-GFPs in NorHA hydrogel with thiol/norbornene ratios of 1,0, 0,45 and 0,12 after 1 and 7 days. Only the cells in the 0,12 sample were stretching out, indicating that the higher degree of crosslinking in the other samples results in a stiffness which is too high to allow the change in cell morphology.

As can be seen in Figure 7.11, only the cells in the 0,12-ratio sample started spreading through the gels and developed the spindle shape, characteristic for ASC. The cells in the other two samples kept round morphology even after 7 days of incubation, similar to the cells in the 2PP cell encapsulation experiments.

7.2.3 Particle Formation

Several samples with NorHA hydrogel contained a high amount of impurities, which reduced the imaging quality (Figure 7.12). These impurities were mostly attached to the glass surface and the top of the printed structures and appeared to be small strands of polymerized material.

Die approbierte gedruckte Originalversion dieser Diplomarbeit ist an der TU Wien Bibliothek verfügbar.
The approved original version of this thesis is available in print at TU Wien Bibliothek.
TU Bibliothek Your knowledge hub WIEN

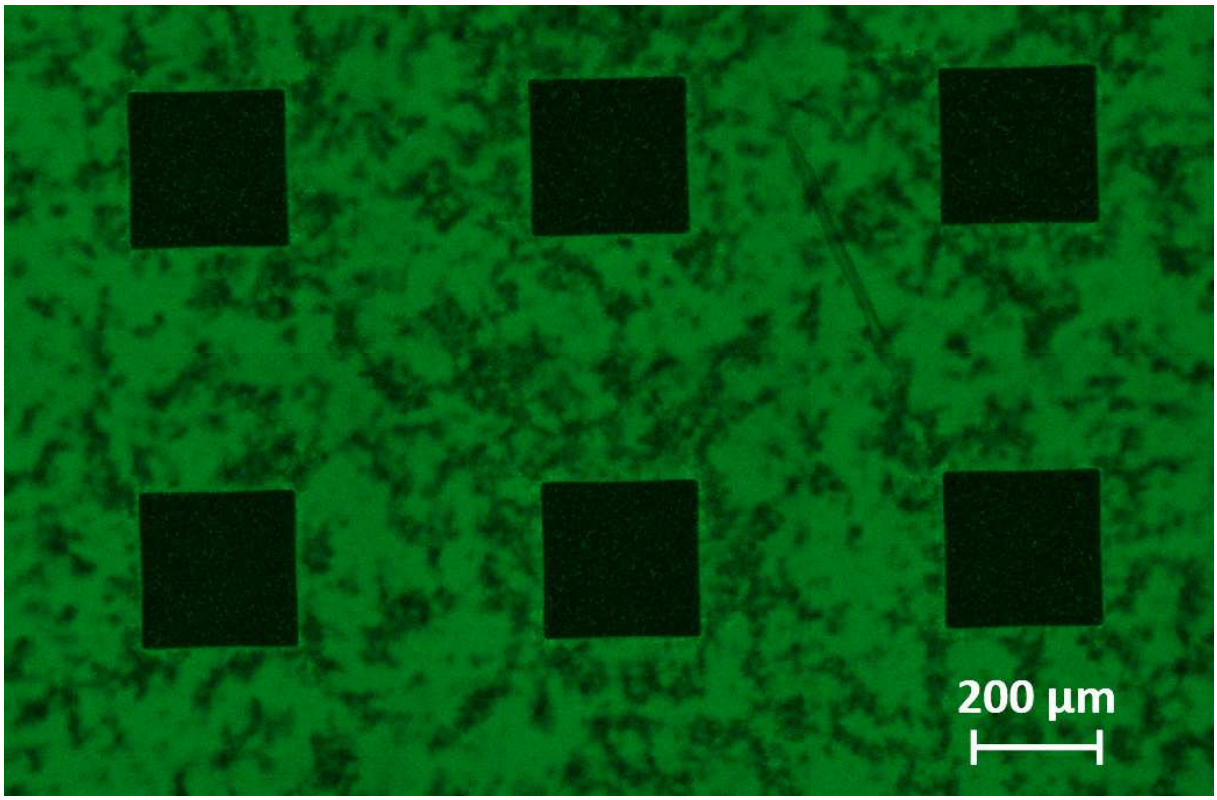

Figure 7.12: CLSM image of printed cubes surrounded by impurities in a NorHA hydrogel sample. These impurities lead to a reduced image quality of the structures and complicate analysis.

Multiple potential reasons were taken into consideration as cause for this behavior:

- Unstable material, which polymerizes without photoinitiation.
- The light sources in the laboratory are equipped with filters to enable the work with photosensitive chemicals. Imperfections of those filters let light with short wavelengths pass.
- The LED that is used to illuminate the sample during the printing process for observation with the CMOS camera.
- Stray light from the laser during the printing process.

To determine the cause of the unspecific cross-linking three samples with non-polymerized hydrogel were prepared and stored under different conditions. To determine if the cross-linking was induced by light sample 1 was exposed to the light of the laboratory, sample 2 to the red LED. As a control and to exclude unstable material as the cause of the cross-linking sample 3 was wrapped in tin foil, blocking any light. After two hours the samples were compared in a bright-field microscope. Sample 1 and 3 showed no contamination, while sample 2 contained the same

Die approbierte gedruckte Originalversion dieser Diplomarbeit ist an der TU Wien Bibliothek verfügbar.
The approved original version of this thesis is available in print at TU Wien Bibliothek.
TU Bibliothek Your knowledge hub WIEN

impurities that were found in previous samples used for printing. Bright field images of all three samples can be seen in Figure 7.13.

This leads to the conclusion that unspecific cross-linking is caused by the red LED mounted above the objective. Turning off the LED during the structuring process helps to prevent this effect and thus improving the overall quality of the sample and the signal to noise ratio of LSM images.

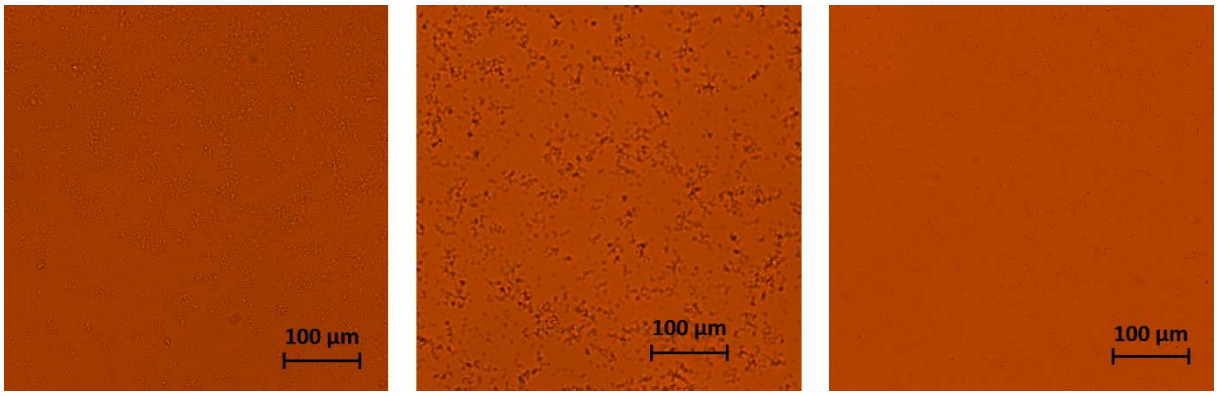

(a) Sample 1: exposed to laboratory light

(b) Sample 2: exposed to red LED

(c) Sample 3: control sample, wrapped in tin foil

Figure 7.13: Bright-field images of the three samples containing unpolymerized NorHA hydrogel, which were used to find the reason for the impurities found in previous experiments. Only sample 2 (b) shows the same impurities, which leads to the conclusion that the red LED mounted above the printer is the cause of the impurities.

Die approbierte gedruckte Originalversion dieser Diplomarbeit ist an der TU Wien Bibliothek verfügbar.
The approved original version of this thesis is available in print at TU Wien Bibliothek.
TU Bibliothek Your knowledge hub WIEN

8 Outlook & Conclusion

The experiments showed that the use of 2PP parameters to influence the stiffness of gelatin- and hyaluronic acid-based hydrogel structures is possible. Laser powers close to the threshold create structures with a smaller percentage of crosslinked material and can therefore be used to build areas with higher cell proliferation. One approach for a practical application of this effect would be to print objects consisting of a shell with higher stiffness and inner parts with low stiffness. This procedure should also enable to build structures with even lower degrees of crosslinking as the softer material would be supported by the stiffer parts.

The experiments in this thesis have proven that the creation of structures from GelNB hydrogel that either allow or suppress changes of cell morphology by means of 2PP is possible. The next step will be to combine those properties into single structures by using more complex designs, with varying power settings.

While the creation of structures from NorHA hydrogel inside which cells can spread out with 2PP has not yet been successful, it has already been shown that this is possible by using UV curing instead and that the stiffness of NorHA hydrogel shows a power dependency as well. Therefore, successful cell encapsulation with 2PP should be possible by using stiffer supporting structures like explained above.

The python program created during the course of this thesis, was built with usability and adaptability for new applications in mind. The use of a GUI and creation of a guide for the whole swelling test procedure should even allow people without programming knowledge to use the program for further material tests. It should easily be possible to use the program to analyze the influence of further parameters on the swelling behavior.

One parameter that is not optimized yet and is expected to have a big influence on hydrogel structures is the layer spacing. On one hand, the layer spacing can increase the manufacturing speed noticeable. On the other hand an increase of the layer spacing at constant power is expected to lead to lower stiffness and could therefore influence the behavior of encapsulated cells.

Die approbierte gedruckte Originalversion dieser Diplomarbeit ist an der TU Wien Bibliothek verfügbar.
The approved original version of this thesis is available in print at TU Wien Bibliothek.
TU Bibliothek Your knowledge hub WIEN

9 Appendix

9.1 Hydrogel preparation calculation sheet

Table 9.1: Exemplary instance of the spreadsheet, which was used for material preparation

NorHA mass	**2**	**mg**
cell media	**0**	**µl**
DS NorHA	30	%
Mw NorHA	415,365	g/mol
desired concentration	4	w/v%
Mol NorHA	4,815	µmol
PBS to add to NorHA	42,71	µl
AS 7 stock concentration	10	mM
AS7 desired concentration	0,5	mM
AS7 stock solution to add	2,5	µl
Thiol:ene ratio	1	
crosslinker valency	2	
Mw crosslinker	154,25	g/mol
crosslinker to add	0,111	mg
Mol Crosslinker	0,722	µmol
crosslinker stock solution to add	2,79	µl
total volume	50	µl

DTT stock solution preparation

Concentration	40	mg/ml
Molar Concentration	259,3193	mM
mass DTT	**3,3**	**mg**
PBS to add	82,5	µl

Mw calculation

Mw HA	379,32	g/mol
Mw NorHA (100%)	499,47	g/mol

- **dark blue:** variable; has to be changed for every experiment;
- **light blue:** variable; only must be changed when different base material will be used or the material composition is changed;
- **dark green:** calculated value; needed for preparation
- **light green:** calculated value; additional information; not needed for preparation

Die approbierte gedruckte Originalversion dieser Diplomarbeit ist an der TU Wien Bibliothek verfügbar.
The approved original version of this thesis is available in print at TU Wien Bibliothek.
TU Bibliothek Your knowledge hub WIEN

10 References

[1] M. C. Cushing and K. S. Anseth, "Hydrogel cell cultures," *Science,* vol. 316, no. 5828, pp. 1133-1134, 2007.

[2] A. Ovsianikov *et al.* "Laser Fabrication of Three-Dimensional CAD Scaffolds from Photosensitive Gelatin for Applications in Tissue Engineering," *Biomacromolecules ,* vol. 12, no. 4, pp. 851-858, 2011.

[3] A. Ovsianikov, J. Yoo, V. Mironov *(eds.)*, "3D Printing and Biofabrication", Berlin: Springer, 2018.

[4] P. Gruber, "Development of a novel wavelength-tunable high-speed 2-photon lithography setup," PhD thesis, Technische Universität Wien, 2018.

[5] J. Torgersen *et al.* "Photo-sensitive hydrogels for three-dimensional laser microfabrication in the presence of whole organisms," *Journal of biomedical optics,* vol. 17, no. 10, p. 105008, 2012.

[6] W. M. Gramlich *et al.* "Synthesis and orthogonal photopatterning of hyaluronic acid hydrogels with thiol-norbornene chemistry," *Biomaterials ,* vol. 34, no. 38, pp. 9803-9811, 2013.

[7] G. Odian, "Principles of polymerization", John Wiley & Sons, 2004.

[8] B. M. Mandal, "Fundamentals of polymerization", 2013: World Scientific.

[9] A. L. Colebatch and A. S. Weller, "Amine–Borane Dehydropolymerization: Challenges and Opportunities.," *Chemistry–A European Journal,* vol. 25, no. 6, pp. 1379-1390, 2019.

[10] J. P. Fisher *et al.*, "Photoinitiated polymerization of biomaterials.," *Annual review of materials research,* vol. 31, no. 1, pp. 171-181, 2001.

[11] D. S. D. Kim *et al.*, "Hydrostatic 3D-printing for soft material structures using low one-photon polymerization.," *Manufacturing Letters,* vol. 10, pp. 6-9, 2016.

Die approbierte gedruckte Originalversion dieser Diplomarbeit ist an der TU Wien Bibliothek verfügbar.
The approved original version of this thesis is available in print at TU Wien Bibliothek.
TU Bibliothek Your knowledge hub WIEN

[12] W. Steiger, "Investigation of Multi-Photon Processing Parameters and Materials," PhD thesis, Technische Universität Wien, 2018.

[13] P. J. Bártolo *(Ed.)*, "Stereolithography: materials, processes and applications", Springer Science & Business Media, 2011.

[14] M. Göppert-Mayer, "Über Elementarakte mit zwei Quantensprüngen.," *Annalen der Physik,* vol. 401, no. 3, pp. 273-294, 1931.

[15] W. Kaiser and C. G. B. Garrett, "Two-photon excitation in Ca F 2: Eu 2+.," *Physical review letters,* vol. 7, no. 6, p. 229, 1961.

[16] F. Gantner, "Fabrication and Evaluation of Brain Phantoms for MRI Calibration utilizing laser-based 3D-Printing Technology.," Master thesis, Technische Universität Wien, 2018.

[17] D. L. Andrews, "Molecular photophysics and spectroscopy.", Morgan & Claypool Publishers, 2014.

[18] R. R. Birge and B. M. Pierce, "Semiclassical time-dependent theory of two-photon spectroscopy. The effect of dephasing in the virtual level on the two-photon excitation spectrum of isotachysterol.," *International Journal of Quantum Chemistry,* vol. 29, no. 4, pp. 639-656, 1986.

[19] S. Ruzin and H. Aaron, "University of California, Berkeley" [Online]. Available: http://microscopy.berkeley.edu/courses/TLM/2P/index.html. [Accessed 05 January 2020].

[20] S. W. Paddock, "Principles and practices of laser scanning confocal microscopy.," *Molecular biotechnology,* vol. 16, no. 2, pp. 127-149, 2000.

[21] N. S. Claxton, T. J. Fellers and M. W. Davidson, "Laser scanning confocal microscopy.," Department of Optical Microscopy and Digital Imaging, Florida State University, Tallahassee, 2006.

[22] J. Van Hoorick *et al.*, "Highly Reactive Thiol-Norbornene Photo-Click Hydrogels: Toward Improved Processability," *Macromolecular rapid communications,* vol. 39, no. 14, p. 1800181, 2018.

Die approbierte gedruckte Originalversion dieser Diplomarbeit ist an der TU Wien Bibliothek verfügbar.
The approved original version of this thesis is available in print at TU Wien Bibliothek.
TU Bibliothek Your knowledge hub WIEN

[23] M. Tromayer *et al.*, "A biocompatible diazosulfonate initiator for direct encapsulation of human stem cells via two-photon polymerization," *Polymer Chemistry,* vol. 9, no. 22, pp. 3108-3117, 2018.

[24] S. R. Caliari, S. L. Vega *et al.*, "Dimensionality and spreading influence MSC YAP/TAZ signaling in hydrogel environments.," *Biomaterials,* vol. 103, pp. 314-323, 2016.

[25] L. Yang *et al.*, "On the Schwarzschild Effect in 3D Two-Photon Laser Lithography.," *Advanced Optical Materials,* vol. 7, no. 22, p. 1901040, 2019.

[26] A. Dobos *et al.*, "Thiol–Gelatin–Norbornene Bioink for Laser-Based High-Definition Bioprinting," *Advanced healthcare materials,* p. 1900752, 2019.

Die approbierte gedruckte Originalversion dieser Diplomarbeit ist an der TU Wien Bibliothek verfügbar.
The approved original version of this thesis is available in print at TU Wien Bibliothek.
TU Bibliothek Your knowledge hub WIEN

11 List of Figures

Die approbierte gedruckte Originalversion dieser Diplomarbeit ist an der TU Wien Bibliothek verfügbar.
The approved original version of this thesis is available in print at TU Wien Bibliothek.
TU Bibliothek Your knowledge hub WIEN

Die approbierte gedruckte Originalversion dieser Diplomarbeit ist an der TU Wien Bibliothek verfügbar.
The approved original version of this thesis is available in print at TU Wien Bibliothek.
TU Bibliothek Your knowledge hub WIEN

12 List of Tables

Die approbierte gedruckte Originalversion dieser Diplomarbeit ist an der TU Wien Bibliothek verfügbar.
The approved original version of this thesis is available in print at TU Wien Bibliothek.
TU Bibliothek Your knowledge hub WIEN

13 Abbreviations

1PA	1-Photon Absorption
2PA	2-Photon Absorption
2PP	2 Photon Polymerization
AFM	Atomic force microscope
AOM	Acousto-optic modulator
ASC	Adipose-derived stem cells
B&W	black and white
CLSM	Confocal laser scanning microscope
CMOS	Complementary metal-oxide-semiconductor
DAS	tetrapotassium 4,4′-(1,2-ethenediyl)bis[2-(3-sulfo-phenyl)diazenesulfonate]; a Photoinitiator
DTT	Dithiothreitol
dZ	Layer Spacing
FITC-Dextran	Fluorescein isothiocyanate–dextran
FOV	Field of View
GelNB	Gelatin–norbornene
GFP	Green fluorescent protein
GUI	Graphical user interface
NA	Numerical aperture
NorHA	Norbornene-functionalized hyaluronic acid
OpenCV	Open source computer vision
PBS	Phosphate buffered saline solution

Die approbierte gedruckte Originalversion dieser Diplomarbeit ist an der TU Wien Bibliothek verfügbar.
The approved original version of this thesis is available in print at TU Wien Bibliothek.
TU Bibliothek Your knowledge hub WIEN